Journal of Rock Mechanics and Geotechnical Engineering xxx (xxxx) xxx

Contents lists available at ScienceDirect

Journal of Rock Mechanics and Geotechnical Engineering

journal homepage: www.jrmge.cn

Review

Advances in joint roughness coefficient (*JRC*) and its engineering applications

Nick Barton [a], Changshuo Wang [b,*], Rui Yong [c]

[a] Nick Barton & Associates, Fjordveien 65c, Høvik, Oslo, 1363, Norway
[b] School of Civil Engineering, Shijiazhuang Tiedao University, Shijiazhuang, 050043, China
[c] Rock Mechanics Institute, Ningbo University, Ningbo, 315211, China

ARTICLE INFO

Article history:
Received 25 October 2022
Received in revised form
15 February 2023
Accepted 21 February 2023
Available online xxx

Keywords:
Joint roughness coefficient (*JRC*)
Rock joints
Roughness
Shear strength
Scale effect

ABSTRACT

The joint roughness coefficient (*JRC*), introduced in Barton (1973) represented a new method in rock mechanics and rock engineering to deal with problems related to joint roughness and shear strength estimation. It has the advantages of its simple form, easy estimation, and explicit consideration of scale effects, which make it the most widely accepted parameter for roughness quantification since it was proposed. As a result, *JRC* has attracted the attention of many scholars who have developed *JRC*-related methods in many areas, such as geological engineering, multidisciplinary geosciences, mining mineral processing, civil engineering, environmental engineering, and water resources. Because of such a developing trend, an overview of *JRC* is presented here to provide a clear perspective on the concepts, methods, applications, and trends related to its extensions. This review mainly introduces the origin and connotation of *JRC*, *JRC*-related roughness measurement, *JRC* estimation methods, *JRC*-based roughness characteristics investigation, *JRC*-based rock joint property description, *JRC*'s influence on rock mass properties, and *JRC*-based rock engineering applications. Moreover, the representativeness of the joint samples and the determination of the sampling interval for rock joint roughness measurements are discussed. In the future, the existing *JRC*-related methods will likely be further improved and extended in rock engineering.

© 2023 Institute of Rock and Soil Mechanics, Chinese Academy of Sciences. Production and hosting by Elsevier B.V. This is an open access article under the CC BY-NC-ND license (http://creativecommons.org/licenses/by-nc-nd/4.0/).

1. Introduction

Rock joints, mechanical discontinuities of geological origin, intersect almost all near-surface rock masses and significantly influence their engineering properties. Roughness is an essential component of the shear strength of rock joints, particularly in the case of undisplaced and interlocked features such as unfilled joints. This is because lack of planarity means dilation, higher local stresses, and increased permeability. Over the past five decades, researchers have proposed different methods to quantify the joint roughness (e.g. Barton and Choubey, 1977; Yu and Vayssade, 1991; Kulatilake et al., 2006; Tatone and Grasselli, 2010; Yong et al., 2017). Among all the joint roughness parameters in the literature, the joint roughness coefficient (*JRC*) is the one most widely used in practice. It was first proposed by Barton (1973) some 50 years ago for evaluating rock joint shear strength and quantifying roughness. *JRC* was later adopted by the International Society for Rock Mechanics (ISRM) (Barton, 1978) for the description of discontinuities. It has the advantages of simple form, easy estimation, and explicit consideration of scale effects. Since the quantification of *JRC* is crucial to the shear strength of jointed rock masses, it has attracted a large number of attentions.

JRC-related methods have gradually developed as general methods for solving rock engineering stability problems. The concept of *JRC* has been applied in various fields such as geological engineering, multidisciplinary geosciences, mining mineral processing, civil engineering, environmental engineering, and water resources. In these *JRC*-related methods, the nonlinear rock joint shear strength criterion, called Barton-Bandis criterion (also called BB criterion), is the most used. This criterion, with the shear strength portion refined by Barton and Choubey (1977), received important additions from the scale-effects and normal-closure work of Bandis (1980). Since the 1980s, this criterion has been used in numerous computer codes for mechanical-hydraulic

* Corresponding author.
E-mail address: changshuowang@foxmail.com (C. Wang).
Peer review under responsibility of Institute of Rock and Soil Mechanics, Chinese Academy of Sciences.

https://doi.org/10.1016/j.jrmge.2023.02.002
1674-7755 © 2023 Institute of Rock and Soil Mechanics, Chinese Academy of Sciences. Production and hosting by Elsevier B.V. This is an open access article under the CC BY-NC-ND license (http://creativecommons.org/licenses/by-nc-nd/4.0/).

Please cite this article as: Barton N et al., Advances in joint roughness coefficient (*JRC*) and its engineering applications, Journal of Rock Mechanics and Geotechnical Engineering, https://doi.org/10.1016/j.jrmge.2023.02.002

coupled modeling (e.g. UDEC-BB since 1985) because it is nonlinear and more accurate than the traditional Mohr-Coulomb linear method.

Since the introduction of the *JRC* concept in 1973, many researchers have sought to find better methods of objectively and accurately estimating *JRC*. Many innovative, impartial, and practical methods were proposed for joint roughness characterization. In these methods, Barton and Choubey (1977) were the first to apply the tilt test (or self-weight gravity shear test) method in a 'scientific' way to determine *JRC*. Some researchers have misunderstood and thought that *JRC* is a subjective parameter that only reflects two-dimensional (2D) roughness and not three-dimensional (3D) roughness. Obviously, the tilt test reflects the "real" 3D shear behavior of rock joints, thus *JRC* recorded in this way is 3D. In addition, the shearing direction is also taken into consideration in the tilt test; thus, the *JRC* records the directional roughness. The authors are aware of numerous different equations for assessing *JRC* (e.g. Tse and Cruden, 1979; Yu and Vayssade, 1991; Tatone and Grasselli, 2010; Kulatilake et al., 2006; and many others). However, the great majority are rather complex descriptions of a topological nature or linked to 3D laser profilometric analysis. For engineering application purposes, the joint roughness characterization method must be quantitative and meaningful, and the cost must remain within acceptable limits. Additionally, when using mathematical descriptions of digitized joint topology, surface weathering (or prior shear) should not interfere with such surface exposure analysis.

This paper consists of the following parts. The next section 2 introduces the origin and early application of *JRC*. Section 3 reviews the roughness measurement of *JRC*. Section 4 introduces the methods for *JRC* estimation. The investigations of anisotropy and scale effect of joint roughness are given in Section 5. In Section 6, we conclude the descriptions of the properties of rock joints based on *JRC*. Section 7 summarizes the influences of *JRC* on the properties of rock masses. Section 8 introduces the engineering applications. Finally, the discussion and conclusions are drawn in Sections 9 and 10, respectively.

2. Origin and connotation of *JRC*

The main purpose of joint roughness quantification is to facilitate the estimation of shear strength, especially for unfilled joints where estimates may be quite accurate.

The following equation related to granular materials was proposed by Newland and Allely (1957) to describe and estimate the shear resistance of sands and granular soils:

$$\tau = \sigma_n \tan(\varphi_b + i) \tag{1}$$

where τ denotes the maximum shear strength, σ_n is the effective normal stress, φ_b denotes the angle of frictional sliding resistance between particles, and i is the average angle of deviation of particle displacements from the direction of the applied shear stress.

Patton (1966) observed that the shear strength of irregular joint surfaces could also be represented by Eq. (1) under low normal stresses. However, the Coulomb linear relation was assumed to be satisfied under high normal stresses because most irregularities were expected to be sheared off. Thus, the following bilinear envelope equation was proposed for describing the shear resistance under both high normal stresses and low normal stresses:

$$\tau = \begin{cases} \sigma_n \tan(\varphi_b + i) (\text{for low normal stresses}) \\ c + \sigma_n \tan \varphi (\text{for high normal stresses}) \end{cases} \tag{2}$$

where c and φ are the Coulomb parameters, i.e. the cohesion and friction angle, respectively.

Patton (1966) found that the "first-order" irregularities provide the predominant contributions to the shear strength of major joint surfaces under natural slopes (Fig. 1a) because "second-order" irregularities usually fail due to slope creep and weathering. Notably, all scales of the roughness of rock joints below the surface-weathered zone are probably significant. Fig. 1b depicts an idealized, smooth, inclined joint surface. Sliding is initiated when the resultant force is inclined at an angle φ_b (basic friction angle) from the normal to the inclined surface. Therefore, the tangent of the "total friction angle" is equal to the ratio of the horizontal force to the normal force acting on the rock joint. However, the surface of a natural joint often has a wide variety of asperities with various i values (Fig. 1c). If this hypothetical sample in Fig. 1c is extracted for shear testing, then the ratio of H and N can be expressed as follows:

$$H / N = \tan(\varphi_b + d_n + s_n) \tag{3}$$

where d_n denotes the peak dilation angle equal to the instantaneous inclination of the shearing path at peak strength relative to the mean plane. This component represents the minimum energy path between a "sliding-up" and a "shearing through" failure mode. s_n is the shear component that represents the failure of surface asperities.

Barton (1971, 1973) originally developed a method of estimating the shear strength of 'fractures' based on experimental observations of the behavior of rough artificial tension fractures which were developed through realistic brittle model materials. The unconfined compressive strengths (σ_c) of the tested samples ranged between 0.072 MPa and 0.84 MPa. Barton (1971) obtained the following empirical equations based on the relationship between d_n and $\tan^{-1}(\tau/\sigma_n)$ and the relationship between d_n and σ_c/σ_n:

$$\tau / \sigma_n = \tan(2d_n + 30^\circ) \tag{4}$$

$$d_n = 10 \log_{10}(\sigma_c / \sigma_n) \tag{5}$$

The criterion of peak shear strength for rough-undulating and unweathered joints could therefore be written as follows:

$$\tau / \sigma_n = \tan[20 \log_{10}(\sigma_c / \sigma_n) + 30^\circ] \tag{6}$$

The values of φ_b for the model materials varied from 28.5° to 31.5°; thus, the value of 30° in Eq. (6) can be viewed as an approximation to φ_b. As joint samples are normally unweathered in their original in situ condition, σ_c in Eq. (6) will yield an upper bound estimate of τ. Following this early work with artificial tension fractures, the effective joint wall compressive strength (*JCS*) was proposed (Barton, 1973) for generalizing both weathered and unweathered joints. If the joints are completely unweathered, *JCS* will equal the unconfined compressive strength of the unweathered rock (σ_c). In general, rock joint walls are weathered to some extent, and the *JCS* will be lower than σ_c.

Since the shear strength measured along individual joints strongly depends on the joint roughness. Eq. (6) can be modified to incorporate different degrees of surface roughness.

To investigate the influence of surface roughness on shear strength, the three estimates shown in Fig. 2 were preliminary efforts to improve the classification and description of non-planar joints (*JRC* = 20, 10 and 5 for classes A, B and C, respectively).

Later, Barton (1973) found that the peak friction angle can be quantitatively represented by *JRC*, *JCS* and φ_b, and the peak shear strength can be expressed in a generalized form based on

Please cite this article as: Barton N et al., Advances in joint roughness coefficient (*JRC*) and its engineering applications, Journal of Rock Mechanics and Geotechnical Engineering, https://doi.org/10.1016/j.jrmge.2023.02.002

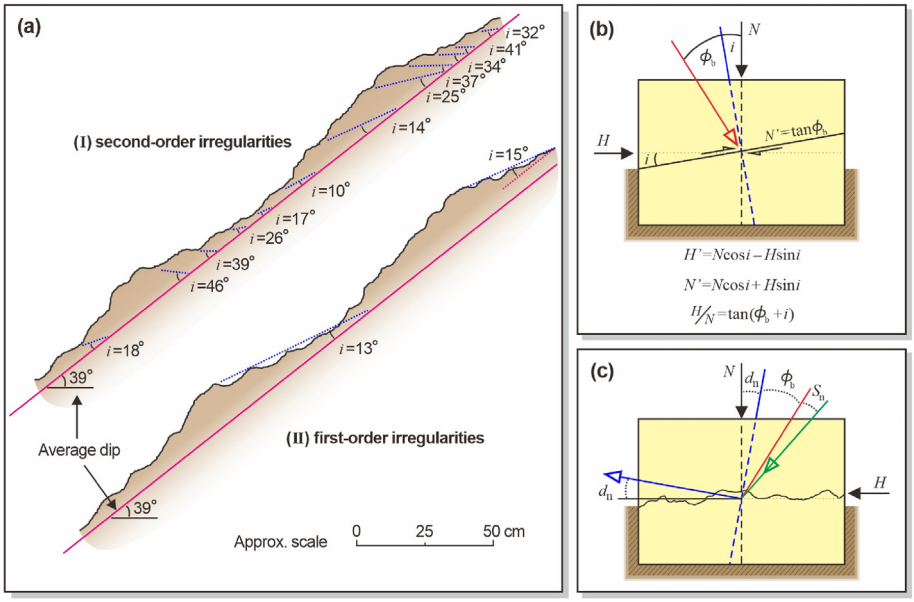

Fig. 1. (a) The effective *i* value for a natural slope under different orders of irregularities (after Patton, 1966); and the angular components of shear strength for (b) a planar joint and (c) a non-planar joint (after Barton, 1973).

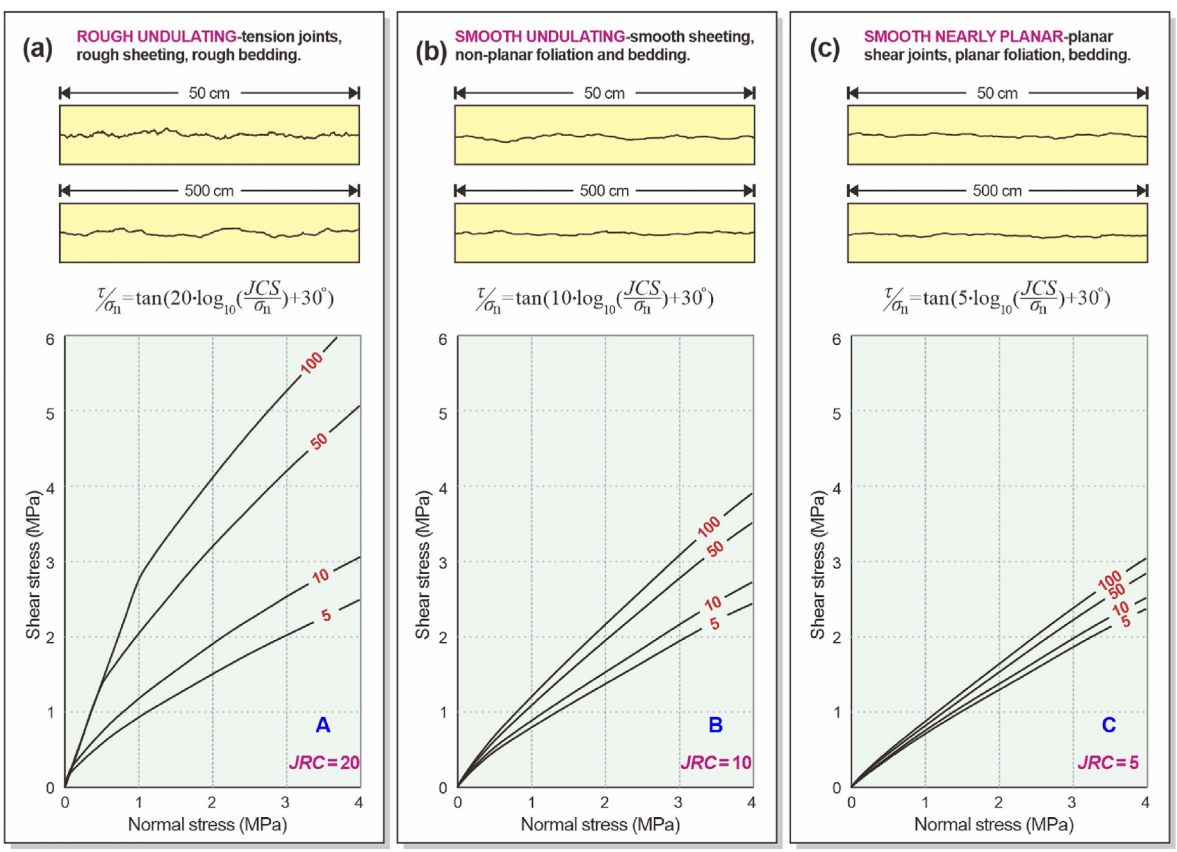

Fig. 2. Empirical law for prediction of shear strength of non-planar joints (after Barton, 1973). (a), (b) and (c) show the roughness profiles as an approximate guide to the appropriate *JRC* values 20, 10 and 5.

laboratory tests of 130 natural joint samples (Fig. 3). The generalized form of Eq. (6) was given as follows (Barton, 1973):

$$\tau / \sigma_n = \tan[JRC \log_{10}(JCS / \sigma_n) + \varphi_b] \quad (7)$$

The '*i*-value' in Eq. (2) can therefore be replaced by a stress-dependent logarithmic function incorporating variable (and scale-dependent) roughness. *JRC* was later defined as a sliding scale of roughness ranging from approximately 20 to 0 from the roughest to

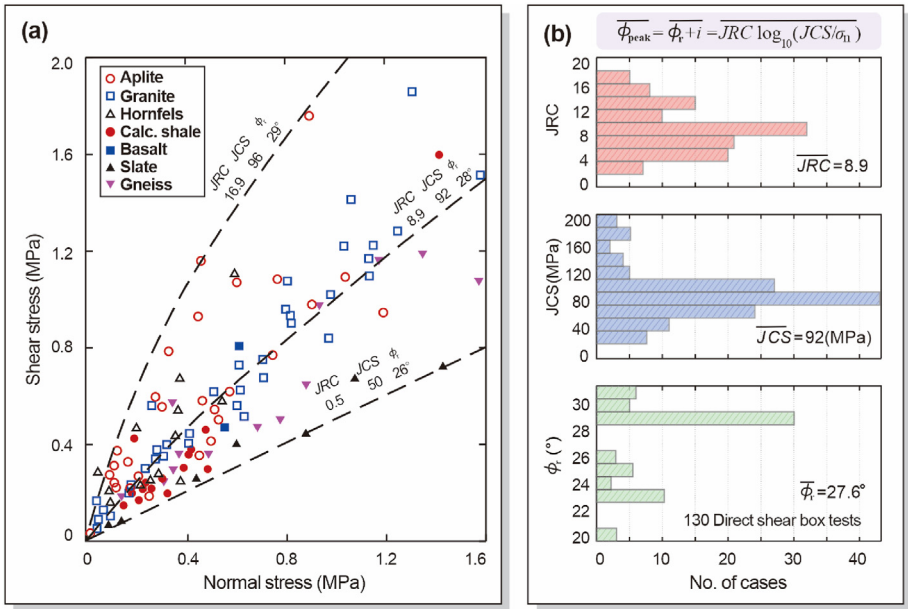

Fig. 3. Peak shear strength and the statistical result of *JRC*, *JCS* and φ_r for 130 natural joint samples based on laboratory tests at 100 mm scale (after Barton and Choubey, 1977).

the smoothest end of the spectrum. It is a dimensionless number, approximately equivalent to the ratio of roughness amplitude and sample length (with a multiplier of approximately 400). It is important to note that the parameter *JRC* describes the relative roughness of rock joint walls which have *correlated* roughness, i.e. there is a considerable degree of potential interlock when the joint is 'closed' by increased normal stress. The *JRC* can be determined by rearrangement of Eq. (7) as follows:

$$JRC = \frac{\tan^{-1}(\tau/\sigma_n) - \varphi_b}{\log_{10}(JCS/\sigma_n)} \tag{8}$$

The suggested parameters, *JRC*, *JCS* and φ_b, were soon expanded to include the residual friction angle φ_r for weathered joints (Barton and Choubey, 1977). The improved empirical model of peak shear strength and the corresponding form of *JRC* for the general case of weathered and unweathered joints is given as follows:

$$\tau / \sigma_n = \tan[JRC \log_{10}(JCS / \sigma_n) + \varphi_r] \tag{9}$$

$$JRC = \frac{\tan^{-1}(\tau/\sigma_n) - \varphi_r}{\log_{10}(JCS/\sigma_n)} \tag{10}$$

JCS can be estimated using the point load test (if the joint wall can be sampled) or the Schmidt hammer index test (Broch and Franklin, 1972; Barton and Choubey, 1977). The parameter φ_b in fact reflects the mineralogical properties of planar rock surfaces. Thus, measuring φ_b requires smooth and unweathered rock surfaces, such as saw cuts or core, both without ridges. Although steep micro-asperities may be displayed on planar rock surfaces under microscopic examination, the planar surfaces should have no obvious roughness component on a visible scale. Therefore, the value of φ_b can be obtained from residual shearing tests on planar rough-sawn or sand-blasted rock surfaces. Generally, the value of φ_b can be estimated from the recommended values for various rock types and moisture conditions reviewed from an extensive literature by Barton and Choubey (1977). Additionally, the value of φ_r can be estimated based on the ratio between the Schmidt hammer rebound *r* obtained on a saturated weathered joint wall and the rebound *R* obtained on an unweathered dry rock surface as follows:

$$\varphi_r = \varphi_b - 20^\circ + 20r/R \tag{11}$$

Since the *JCS* and φ_b (or φ_r) values can be estimated quite accurately, the real unknown is the *JRC*. Detailed information regarding *JRC* estimation methods is discussed in Section 4, and some properties of joint roughness investigations based on *JRC* are discussed in Section 5.

3. Roughness measurement for *JRC*

In general, *JRC* can be obtained based on two options: roughness measurement-based estimation and actual testing techniques (the details are given in Section 4). Accurate measurement of the roughness of the rock joint surface may be drill-core based or utilizing unweathered exposures if these are available. This section presents some commonly used instruments and methods to measure joint roughness in situ and in the laboratory. It is noticed that joint roughness measurement continues to gain attention as high-performance computing and non-contact measurement techniques become more widespread. These methods (e.g. photogrammetry, image processing, structured-light scanning, and laser scanning) provide good solutions for roughness measurement-based *JRC* estimation. Photogrammetry refers to the process of measuring 3D information from two or more 2D images of the same scene taken from different standpoints (Buzzi and Casagrande, 2018; Bahaaddini et al., 2022). The image processing method for roughness measurement is the image recognition technology to quantify surface roughness. But unlike photogrammetry, it does not need to obtain the 3D topography of the discontinuity surface (Krohn and Thompson, 1986; Bae et al., 2011). A structured-light scanner is a 3D scanning tool that uses projected alternating stripes and a camera system to compute an object's 3D geometry (Grasselli, 2001; Liu et al., 2017a). In comparison to other 3D scanning techniques, it has a number of benefits, including portability, high accuracy, fast speed, and a preference for small to medium-sized objects. Laser scanning method for roughness measurement is based on measuring the distance to the object using lasers according to the speed of light (Fardin et al., 2001, 2004; Lee et al., 2001; Fardin, 2008; Ge et al., 2014; Zheng et al., 2021). A pulsed

beam of light is emitted, and the time it takes to return after reflecting off some surface is measured and used to calculate the relative distance to that surface. Additionally, based on the statistical information of joint surfaces measured by the above-mentioned method, some researchers did productive work on the reconstruction of rock joints (Ficker and Martisek, 2016; Nie et al., 2019; Liu et al., 2022). However, given the length of the paper, these non-contact methods are only briefly introduced as above.

3.1. Profile combs

Barton and Choubey (1977) used a commercially available but high-quality device (Fig. 4a) that allowed a large number (4 per mm) 0.25 mm thin steel shims to perfectly fit the surface of the joint surface along three chosen directions and locations (at 1/4, 1/2 and 3/4 of the sample width) across their joint planes, giving 390 profiles for 130 joint samples. Fig. 4b shows an example of the operation of a profile comb. A small amount of force will overcome the friction between the plates and the pins (as typically found in simpler devices) so that the complete array of pins can be pushed against an irregular surface and adjusted to fit the joint profile. It should be noted that Barton's and Choubey's device did not have the assumed 1 mm resolution with 'steps', but consisted of flat stainless steel metal shims, approximately 4 per mm. It means that the resolution of this device is 0.25 mm instead of 1 mm assumed by many researchers. Yong et al. (2018) proved that this resolution is sufficient for the measurement of joint roughness. When a larger sampling interval is used, measured joint surfaces generally tend to be smoother and the information about the subprime irregular undulations between smaller horizontal spacing may not be efficiently collected. Later, to facilitate the quantification of *JRC*, Özvan et al. (2014) developed a profile digitization process that converts recorded profiles into image files and extracts coordinates based on the actual length of the profile. Hencher and Richards (2015) noted that these typical devices and methods are sufficiently precise for recording and characterizing the overall nature of joints for geological and geotechnical characterization. However, the measurement range of this type of device generally cannot exceed 400 mm. It has significant limitations in determining the roughness of larger-scale profiles.

3.2. Roller and stylus profilometers

A mechanical profilometer usually consists of a stylus or small roller placed in direct contact with a rock joint surface and moved laterally over it. As the stylus or roller is moved laterally, the topography of the surface causes the stylus to be displaced vertically. For this method, the accuracy of the measurement is usually influenced by the diameter of the stylus/roller and the stick-slip motion of the needle on the surface. It is a useful method but can damage weak joint surfaces during measurements. Mechanical profilometers are commonly used for estimating small-scale joint roughness, and the traces of these linear profiles typically exhibit a basic size of a few centimeters (Fig. 5a and b).

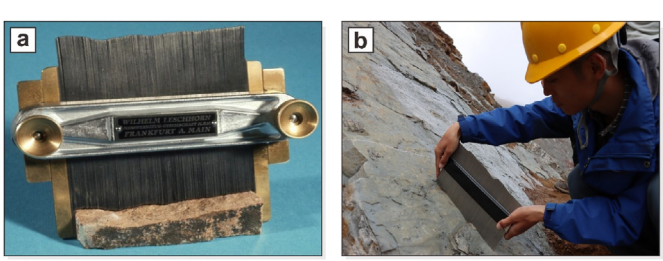

Fig. 4. Joint roughness measurement using the profile combs: (a) High-quality gauge used by Barton and Choubey (1977), and (b) The operation of a profile comb.

The profilometers have also been successfully used to carry out measurements under field conditions (Fig. 5c), albeit less conveniently. To facilitate the measurement, Du (1992) developed a simple mechanical hand profilograph for measuring large-scale rock joint profiles in the field (Fig. 5d). This instrument has the advantages of simple principles of operation, its lightweight, and the continuous roughness-profile drawing. Furthermore, the curve can be obtained quickly, and the measurement length can be extended by adjusting the length of the fixed board. Using this profilograph, the maximum length of the natural joint profiles he measured in the field exceeded 7 m long. The measurements were carried out on a tufa joint in Lin'an, Zhejiang Province, China. To facilitate the quantification of *JRC*, the measured joint profiles need further digitization. Yong et al. (2017) proposed the grayscale image processing technique for digitizing joint profiles. Based on this technique, the obtained profile coordinates have high precision (the measuring error was negligible at approximately 0.1 mm) and can be acquired with flexible sampling intervals. In addition, the largest obstacle to applying this technique in the field is the location of the exposed rock joints, which should be accessible and have enough space for measurement.

3.3. Straight edges and rulers

The dilatation behavior is highly dependent on the asperity amplitude, and the maximum amplitude usually plays the most important role in controlling the shear strength of rock joints. For field estimates of *JRC*, Barton (1981) proposed the relations between the *JRC* and the maximum amplitude (a_{max}) measured over a sample length (L). The value of a_{max} can be measured using a straight edge that is placed on the exposed rock joint surface along a length of L.

Ideally, the edge length should be the same size as the joint. However, considering the limitations and difficulties of roughness measurement in field conditions, it is seldom possible to observe or measure the full length of the joint; as a result, the determination of undulations is often simplified (Piteau, 1970). The orientation of the edge, together with the maximum amplitude, should be recorded. The simplified undulation can be calculated as

$$U = \frac{a_{max}}{L} \tag{12}$$

Due to the time-consuming nature of the measurement in Fig. 6a, the joint waviness can be roughly assessed from visual inspection. To improve the measurement process, Du et al. (2022a) provided a programmed method for determining the maximum amplitude of asperities. Fig. 6b shows a flowchart outlining the stages in determining a_{max}. It has been verified that this method can effectively estimate the *JRC* value of rock joints at the field scale. Based on the acquired amplitude of asperities for individual lengths between straight-edge contact points, Barton (1981) was the first to show how the *JRC* value could be estimated for a wide range of block sizes using a straight edge. This method is introduced in Section 4.

4. Estimation of the *JRC*

4.1. Visual comparison methods

Barton and Choubey (1977) while illustrating the range of rock joint surfaces they had tested, produced the unintended subjective

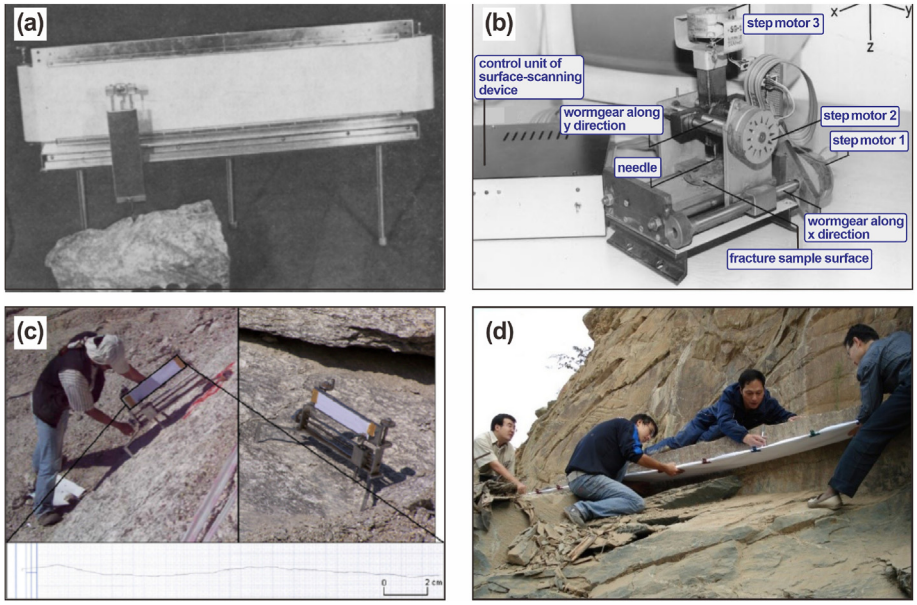

Fig. 5. Joint roughness measurement in the laboratory and in the field using the profilometers: (a) The profilometer developed by Imperial College, U.K. (after Ross Brown and Walton, 1975); (b) A mechanized computer-controlled profilometer (after Develi et al., 2001); (c) A manual profilometer for field use (after Tanyas and Ulusay, 2013); and (d) A mechanical hand profilograph developed by Du (1992) for the roughness field measurement of rock joints several meters in length.

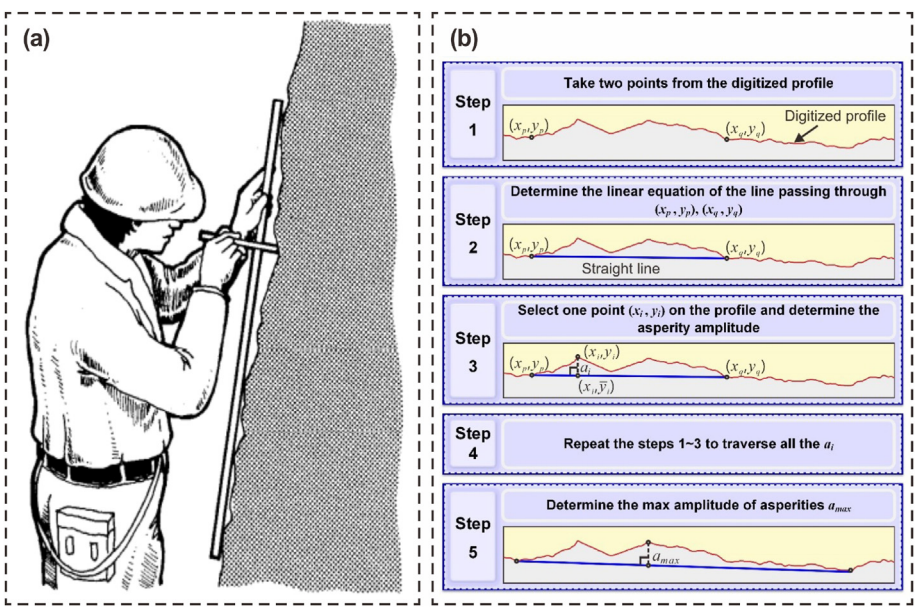

Fig. 6. Joint roughness measurement using straight edges and rulers (a) measuring joint trace amplitude (after Milne et al., 1991), and (b) flowchart illustrating the steps involved in a_{max} determination (after Du et al. 2022a).

method to estimate the *JRC* of a measured profile. They characterized and tested 136 natural rock joints from seven different rock types, and in each case, three profiles were measured for each specimen. The *JRC* values back-calculated from shear box tests were classified into the subsequent ranges: 0–2, 2–4, etc., up to 18–20. Wherever the mean joint plane was not inside $\pm 1^\circ$ of horizontal once placed within the shear box, the shear strengths and corresponding *JRC* values were corrected to the horizontal plane. An effort was then made to pick out the most typical profiles of every cluster. As a result, ten typical profiles were selected from 390 profiles (three per specimen). To assign an approximate *JRC* value to a joint, the measured profile can be visually compared against the typical profiles, as shown in Fig. 7. Note that only rough guidance on likely *JRC* value ranges can be provided by the typical profiles, and there are no decimal places. In fact, the ten typical profiles, with suggested *JRC* ranges, e.g. 8 to 10 and 14 to 16, just illustrate the range of surfaces tested. There are 380 other roughness profiles since there were three per specimen. The main focus was the accuracy of the peak shear strength prediction.

The visual comparison method is in fact suggested by the ISRM to characterize the small-scale roughness of rock joints (Barton, 1978). However, as some researchers are concerned, the visual comparison method is subjective and may cause biases in the *JRC* estimates. For example, Beer et al. (2002) performed a survey based

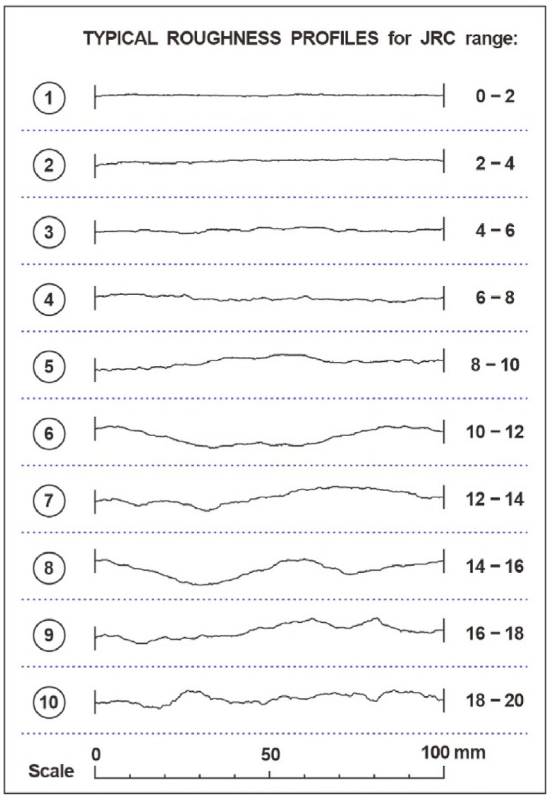

Fig. 7. Typical roughness profiles for the *JRC* range (Barton and Choubey, 1977).

on three granite block profiles with 125, 124 and 122 answers using an internet-based survey system to analyze the reliability of this visual comparison method. The result showed that the JRC mean value and standard deviation varied significantly until the sample size exceeded 50 people. Alameda-Hernández et al. (2014) performed a similar visual estimation survey in consideration of the knowledge and skill of the evaluators. Based on 12 test profiles, 74 undergraduate students, 9 post-graduate students, and 6 experts showed standard deviations of *JRC* values ranging from 1.6 to 3.5, 0.3 to 3.9, and 0.6 to 3.4, respectively. Although the accuracy of *JRC* estimated by the visual comparison method can be improved by increasing experience and the number of people, the precision for problematic profiles, such as profiles not similar with the typical profile, stepped profiles, and profiles showing some similarity with one of the typical profiles but including different roughness amplitudes, can be seen to break down (Beer et al., 2002; Alameda-Hernández et al., 2014). Many efforts have been made to facilitate the application of visual comparisons to accurately estimate *JRCs*, and to reduce the subjective judgment of testers (Milne et al., 2009; Yong et al., 2017; Wang et al., 2019, 2019nlüsoy and Süzen, 2020). Since the essence of the visual comparison method is to assess the similarity between the target profile and typical profiles, image recognition, and deep learning techniques may be utilized to potentially estimate the *JRC* more accurately.

4.2. Experimental methods

4.2.1. Direct shear tests

The typical direct shear test results are shown in Fig. 8a. One may use joint samples with nearly circular (or elliptical) shapes prepared from the core, or samples with square (or rectangular) shapes prepared from sawn blocks, to perform direct shear tests. It is strongly recommended that both adequate and representative samples be recovered from each joint set of relevance. Multiple testing of the same sample must be avoided. In the case of the latter testing procedure, the effective 'friction' of the joint specimen tends to be gradually decreased because of the accumulation of damage with successive shearing of the same joint specimen. As Barton (2013) discussed, the multiple testing of the same sample tends to obtain an artificial 'cohesion' value because the strength envelope is slightly rotated ('clockwise'). Through performing direct shear tests, the shear stress versus displacement and dilation versus displacement curves can be obtained (similar to the sketches in the middle of Fig. 8a). The bottom of Fig. 8a shows typical 'peak' and 'ultimate' strength envelopes. These envelopes will tend to be curved for rough joints. Based on the direct shear test results, the

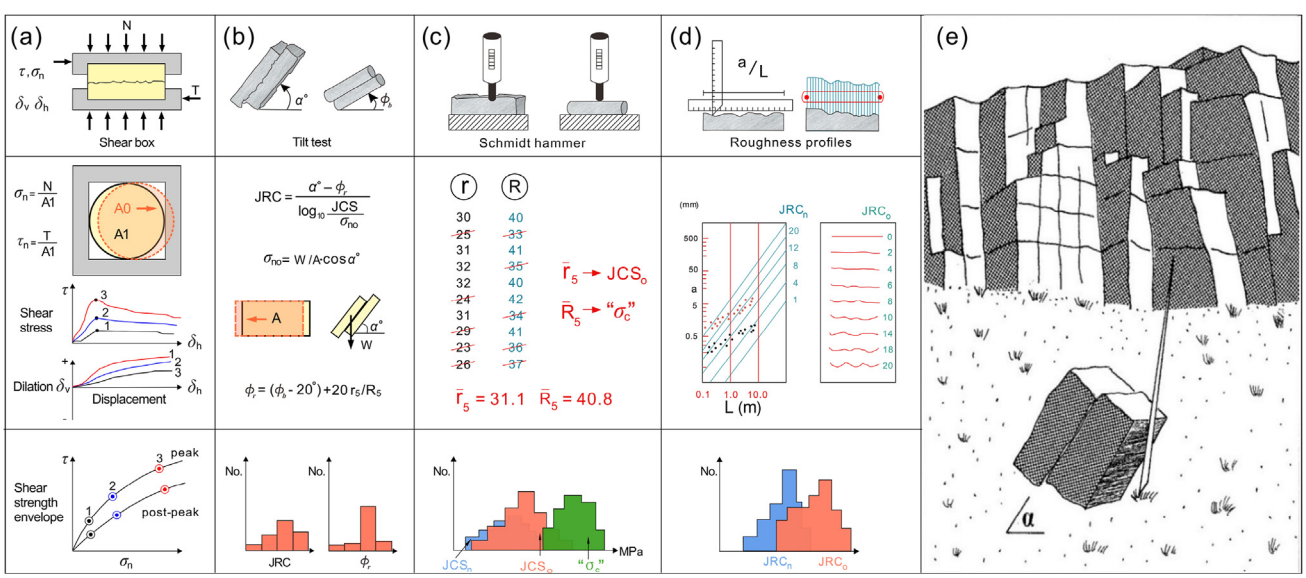

Fig. 8. (a) Typical direct shear test results (Note: avoid moment: use in-line shear forces); (b) Tilt test for *JRC* and φ_r estimates; (c) Schmidt hammer testing for *r* (weathered joint) and *R* (unweathered core stick); (d) JRC measurement using the amplitude/length (*a*/*L*) method, or brush-gauge recording; and (e) Ideally use natural block size to perform tilt test (after Barton, 2013).

Please cite this article as: Barton N et al., Advances in joint roughness coefficient (*JRC*) and its engineering applications, Journal of Rock Mechanics and Geotechnical Engineering, https://doi.org/10.1016/j.jrmge.2023.02.002

JRC values can be estimated by back-analyzing the test results through Eq. (10). It should be noted that $\arctan(\tau/\sigma_n) = 70°$ was a conservative suggested maximum allowable total friction angle for back-calculating the *JRC* based on direct shear tests (Barton and Choubey, 1977).

4.2.2. Tilt tests

Fig. 8b and e illustrates the tilt test performed on a rough joint. When sliding occurs, we can obtain a tilt angle (α). The value of α will be larger than φ_r due to the geometrical effect of roughness. Theoretically, the α follows a simple relationship:

$$\alpha = \arctan(\tau_0 / \sigma_{n0}) \tag{13}$$

where τ_0 is the shear stress and σ_{n0} is the normal stress acting on the joint.

Considering that the length-scale of specimens used to conduct tilt tests is not infinite, Barton and Choubey (1977) used the following empirical relation to estimating σ_{n0}:

$$\sigma_{n0} = \gamma b \cos^2 \alpha \tag{14}$$

where b is the thickness of the top half of the joint (m).

Then, the *JRC* can be estimated by substituting the values of α, σ_{n0} and φ_r into Eq. (15):

$$JRC = \frac{\alpha - \varphi_r}{\log_{10}(JCS/\sigma_{n0})} \tag{15}$$

In fact, the normal stress acting on the joint is uneven. When tilt tests are performed on rock joints with significant roughness, overturning failure may be encountered. Eq. (14) somewhat accommodates the unequal stress distribution while barely impacting the *JRC* calculation. More importantly, it automatically restricts the tilt test to joint surfaces that are 'smooth' enough to avoid overturning failure. Fig. 9 presents the range of applications of tilt tests for estimating *JRC* values (Barton and Choubey, 1977) based on three realistic values of φ_r. Two values of b were assumed: 20 mm for laboratory samples (green curve) and 200 mm for field joints (red curve). The value of *JCS* discussed here is 100 MPa. The curves (red and green) in Fig. 9 were evaluated by Eq. (14). Fig. 9 shows the maximum value of the *JRC* that can be obtained from the tilt tests decreases with increasing φ_r. Taking the test of Barton and Choubey (1977) as an example (the mean of φ_r was 27.5°), the laboratory scale tilt testing can provide a maximum value of *JRC* of roughly 8. The limiting *JRC* value will be at least 10 if field-scale tilt tests are conducted on heavily weathered joints ($\varphi_r = 20°$), especially if the *JCS* value is low because of weathering effects. Given that smoother joints are the primary source of stability issues, the aforementioned tilt test limits frequently will not be significant.

4.2.3. Push or pull tests

The *JRC* values of rougher joints can be estimated using the 'push' or 'pull' tests. In the tests, a joint's upper half is pushed or pulled parallel to the joint plane while the bottom half is positioned horizontally. The weight of the upper half of the joint is the only additional typical load in this situation. Employing this test, the *JRC* of rougher joints can be reliably obtained. The approximate range of *JRC* that may be examined using 'push' or 'pull' tests is shown by the stippled lines in Fig. 9. As presented by Barton and Choubey (1977), the maximum *JRC* value for the 136 specimens with a mean φ_r value of 27.5° that could be satisfactorily obtained with the push or pull tests was approximately 12. The *JRC* value of joints as rough as *JRC* = 20 can be safely determined by doing field 'push' or 'pull' tests on larger and more weathered joints (in this instance, the JCS/σ_n may be as much as two orders of magnitude lower). Therefore, utilizing a combination of tilt and 'push' or 'pull' tests, it should be feasible to quantify the whole range of joint roughness. Additionally, JRC is essentially a constant for a given joint since it does not appear to vary significantly even over a stress range of up to *five* orders of magnitude (Barton and Choubey, 1977). Other studies by Barton (1976) have indicated that this extrapolation may also be performed for very rough joints and over a stress range of up to *eight* orders of magnitude, spanning the whole brittle range of behavior.

4.3. Amplitude/length (a/L) methods

Visual comparison and experimental methods can be used to estimate the *JRC* for profiles within the laboratory scale (i.e. 100 mm). However, rock joints in the field, *or more correctly rock block sizes in the field,* will usually be longer than 100 mm 'Rock block sizes in the field' is emphasized here due to the results of biaxial shear tests on assemblies of fractured blocks of widely different sizes. These exhibited scale effects will be shown in Section 7.1. In this case, a scale-corrected *JRC* should be estimated for large-scale exposures of the relevant joint set. Based on the analysis of some 200 roughness profiles measured on 0.06 m and 0.1 m long and many times longer joint samples (Barton and Choubey, 1977; Bandis, 1980; Bandis et al., 1981), thus including the tests on model replicas of joints of different roughness, the following approximate relationships were proposed to estimate the scale-corrected *JRC* by Barton (1981):

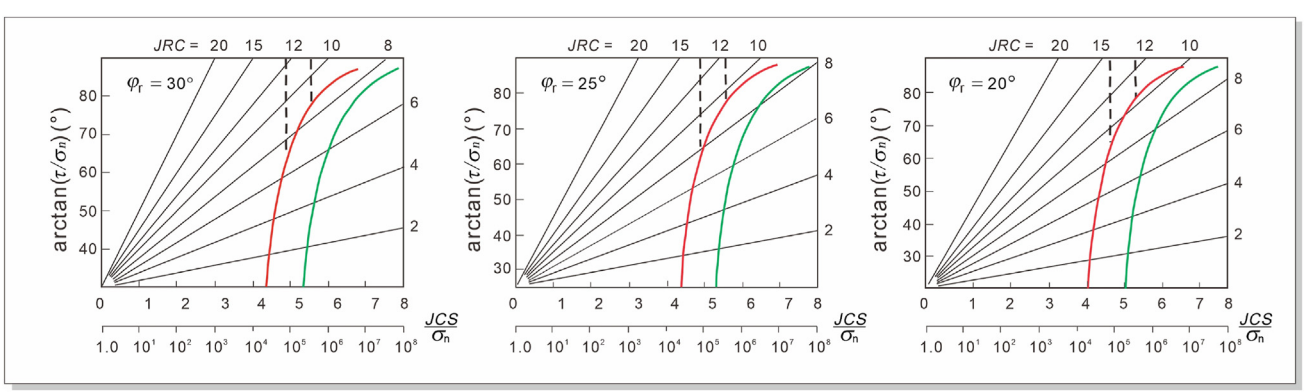

Fig. 9. Range of application of tilt tests and push/pull tests for determining *JRC* values of joints (after Barton and Choubey, 1977).

Please cite this article as: Barton N et al., Advances in joint roughness coefficient (*JRC*) and its engineering applications, Journal of Rock Mechanics and Geotechnical Engineering, https://doi.org/10.1016/j.jrmge.2023.02.002

$$JRC \approx \begin{cases} 400a/L(\text{for } L = 0.1\text{m}) \\ 450a/L(\text{for } L = 1\text{m}) \\ 500a/L(\text{for } L = 10\text{m}) \end{cases} \quad (16)$$

where a is the maximum amplitude measured over a joint sample, and L is the sample length.

Based on the relationships presented in Eq. (16), Barton (1981) developed a simple straight-edge method, as shown in Fig. 10. Through the straight edge method, values of the maximum amplitude (a) measured over a sample length (L) of 0.1 m or up to 1 m and occasionally up to several meters can be used to obtain a rough estimate of the *JRC* at the appropriate scale. Note that in practice, when laying a straight edge along a joint plane, there may be intermediate contact points for the straight edge and correspondingly smaller amplitudes. These should all be recorded, making a 'cloud' of results (representing roughness variation at different scales). The diagram is then used to extrapolate the approximate *JRC* value for the desired block size. *Block size* is given by the mean spacing of joints crossing the joint in question.

Du (1993) examined the straight edge method using the statistical data of the *JRC* measured from rock joints in Xiaolangdi, China. These researchers pointed out that the measurement accuracy of the straight edge method is sufficient to meet the requirements of *JRC* estimates for the surface morphology of rock joints with undulations on the order of millimeters. In addition, the straight edge method has the advantages of being simple and fast. These co-workers also found that the *JRC* in engineering practice can sometimes be greater than 20. This was also found in measurements of a rough bedding plane in limestone at the Karun IV arch dam in Iran. Maximum smaller-scale values of *JRC* of up to 30 were suggested, but when extrapolated to 2 m block sizes, *JRC* was 11. Because of the sometimes larger *JRC* values, Du et al. (1996) proposed a modified straight-edge method (Eq. (17)):

$$JRC = 49e^{29L_0/450L} \arctan(8a/L) \quad (17)$$

where L_0 is the sample length of a joint at the laboratory scale (100 mm).

Considering the small angle approximation $\tan(i) = i$ (herein, the angle i equals $8a/L$), Eq. (17) implies that JRC is equal to 400–500 times the overall angle of inclination associated with the highest amplitude (i.e. 'first order') asperity of the joint. Thus, in a logical conclusion, Eq. (17) implies that *JRC* might be directly proportional to the first-order asperity angle. It should be noted that *JRC* is a mechanical parameter that describes the contribution of surface roughness and undulation to the shear strength of joints. It is a very important parameter in the BB criterion. In this criterion, JRC is not equal to the dilation angle or friction angle, but its effect on shear strength is related to *JCS* and σ_n. Additionally, the first-order roughness (waviness) and the second-order roughness (unevenness) mutually govern the joint mechanical behavior. The estimation of *JRC* values by 'a/L' approach is a simplified strategy based on the assumption that the shear strength of rock joints can be estimated approximately from the first-order roughness. Although the shear strength is mainly governed by the first-order roughness, different-order asperities are involved in the shear process. We have to admit that previous studies have commonly emphasized the relationship between the rock joint shear strength and the overall roughness. In the future, more attention should be paid to the accurate prediction of joint shear properties based on the quantitative evaluation of independent contributions of waviness and unevenness.

To estimate the *JRC* values of joints with laboratory scales, Du et al. (2009) proposed a *basal roughness ruler*. As shown in Fig. 11, the *effective length* and *width* of the ruler are 10 cm and 1.5 cm, respectively. This ruler is manufactured from 3 mm thick biological glass. On the left side of the ruler is noted the amplitude of a joint profile Ry_0. The appropriate *JRC* value of a joint with laboratory scale (JRC_0) is shown on the right side of the ruler.

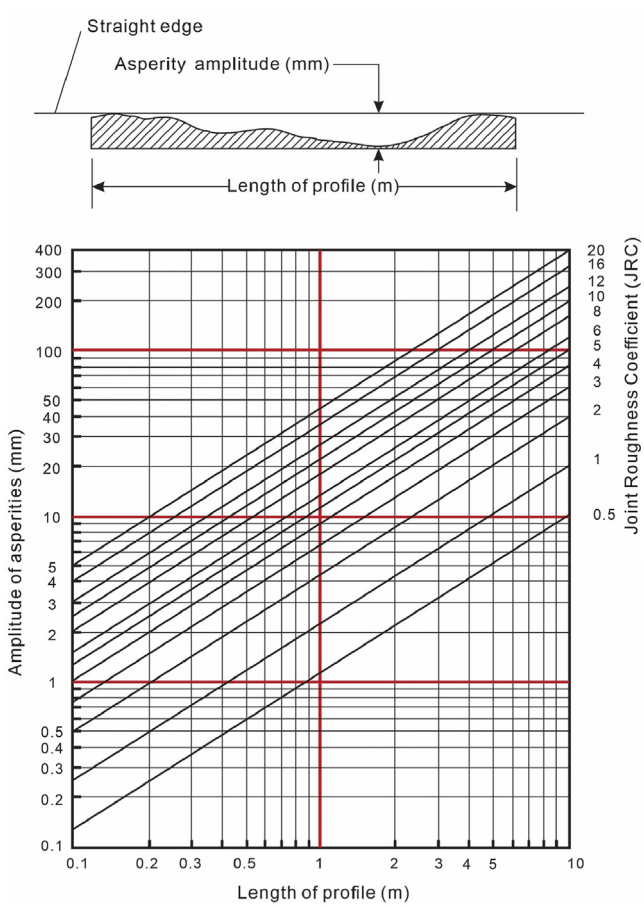

Fig. 10. Joint roughness amplitude/length on various measurement lengths provides estimates of *JRC* when extrapolated to the desired mean block length (from the mean spacing of cross-joints). This may be of a larger dimension than the available straight-edge lengths (after Barton, 1981).

4.4. Summary

Until now, the visual comparison, experimental (particularly the tilt test), and amplitude/length (a/L) methods are the most practical and readily available methods for estimating the *JRC*. Among them, tilt testing and a/L methods are recommended in engineering practice because the visual comparison method is inevitably subjective (Barton and Bandis, 2017). Additionally, the statistical and fractal theories have been introduced to *JRC* estimations (e.g. Tse and Cruden, 1979; Yu and Vayssade, 1991; Kulatilake et al., 2006; Tatone and Grasselli, 2010; and many others). The statistical and fractal methods rely on establishing relationships between the *JRC* and statistical parameters or fractal dimensions. For example, there is a strong correlation between the *JRC* and the standard deviation of the inclination angle, SD_i (Yu and Vayssade, 1991). Pre-*JRC* development, the importance of SD_i and its close resemblance to peak dilation angles when shearing rough tension fractures were demonstrated in Barton (1971) (see also Seidel and Haberfield, 1995). Both the self-similar and self-affine fractals have been suggested for quantifying rock joint roughness. However, rock joint

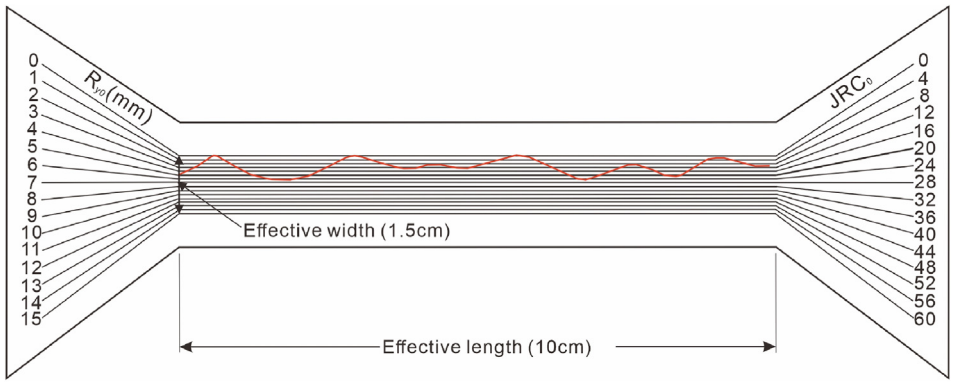

Fig. 11. A basal roughness ruler for the measurement of JRC_0 of profiles with 10 cm (after Du et al., 2009). Ry_0 is the amplitude of a joint profile, and JRC_0 is the *JRC* value of a joint with a laboratory scale.

surfaces are self-affine. Thus, problems are encountered when self-similar methods are used in the calculation of fractal dimensions for self-affine rock joints (Kulatilake et al., 2006, 2021). With the development of computer technology and increased *JRC* databases, artificial intelligence (AI) methods, such as artificial neural networks, support vector machines, and random forests, have been adopted to estimate the *JRC* (Wang et al., 2017). The ability of AI to solve nonlinear problems and the efficiency of AI with regard to *JRC* predictions have promoted the accurate estimation of *JRC*. However, many of them concentrate on the exclusive use of 3D-laser profiling of roughness, and may be omitting certain crucial shear behavior features by never performing (3D) tilt tests while correctly criticizing the over-simplified 2D roughness profiles. The tilt test used for estimating *JRC* is a back-analysis method incorporating two other parameters from the Barton (1973) shear strength criterion: *JCS* and φ_r. This cannot of course apply to 3D surface scanning methods in general, unless relating back to profiles linked to shear strength. When focusing on the various mathematical links between 3D laser scanning of roughness and the 'ten standard (2D) profiles' of Barton and Choubey (1977), potential developers and users should be aware of the implicit 'presence' of the other two parameters in the approximately representative profiles.

Some recommendations for JRC in engineering applications are listed below:

(1) The *JRC* joint roughness coefficient is part of a three-parameters shear strength and joint behavior criterion (involving *JRC*, *JCS* and φ_r) that allows for estimation and extrapolation of shear strength, dilation, normal stiffness and also allows for joint aperture estimation if Lugeon tests have been performed. Scaling rules for the known effect of block size were formally available after the contributions of Bandis in 1980, who also was responsible for the highly nonlinear normal closure formulations using *JRC* and *JCS*.
(2) As is well known, there is considerable subjectivity when using only 2D profiling, and eventual anisotropy is limited by the direction of the measured profile. Clearly, profiling in the adverse (stability-dependent) direction is advised, as would also be needed in the case of preparing samples for tilt-testing. This will often be down-dip since adverse shear stress is the focus. In the case of dam abutments, net effective thrust directions need to be considered.
(3) A recommended approach is to sample the joints of relevant joint sets by recovery in good-quality drill-core, with frequent use of a diamond saw to help form slender jointed samples. These are less likely to topple before sliding in self-weight (gravity-loaded) tilt-test angles, which are typically in the range 50°–75°. Index tests as shown in Fig. 8 are recommended for estimating *JCS* and φ_r.
(4) Scale effects can be allowed for by using the representative block size which is given by the mean spacing of cross-joints. In a realistic UDEC-BB model, each set is likely to have different scaling ratios L_n/L_0, where L_0 represents the representative length of the tilt tests performed, separated into different sets. L_n represents the relevant block sizes (i.e. respective mean spacings of cross-joints).
(5) There are typically kilometers, tens of kilometers, sometimes hundreds of kilometers of core in moderate-scale tunnel, hydropower, dam and mining projects. There should not then be the necessity of *multi-stage shear testing*, which artificially increases the (M – C) cohesion component and reduces the (M – C) friction angle. Tilt testing, though repeated several times to obtain mean values, is not adversely damaging the sample as in the case of *multi-stage shear testing* as normal stresses when sliding occurs in a tilt test may be as low as 0.001–0.002 MPa.

5. Investigation of the anisotropy and scale effect of joint roughness based on the *JRC*

5.1. Anisotropy

In the title of their paper, Barton and Quadros (2015) stated that 'anisotropy is everywhere' in rock engineering, and anisotropic behavior is widespread because of the combined effects of anisotropic structures. Rock joints are formed through diverse, complex fracture mechanisms; this, coupled with the general complexities of rock masses, results in the significant anisotropy of rock joint surfaces. The variation in the joint roughness with respect to different orientations has been recognized as an important source of anisotropic behaviors in rock joints (e.g. Jing et al., 1992; Bae et al., 2011; Yan et al., 2020; Yong et al., 2020).

Diaz et al. (2017) investigated roughness anisotropy based on the *JRC* values of different orientations and suggested a method that can describe the roughness anisotropy of square as well as irregular sampling areas. Rock joints are produced by the action of stress: shear stress and tensile stress, and extension strain (Barton and Shen, 2018). Therefore, rock joints can be divided into two types: shear joints and tensile joints. Shear joints usually extend far along the strike, their attitude occurrence is relatively stable, and their surfaces are relatively planar. The extents of the tensile joints tend to be shorter, their attitude occurrence is often variable, and their joint surfaces tend to be rough at a small scale unless developed when there is strong stress anisotropy (Olson and Pollard, 1991).

However, extension fracturing due to an adverse ratio of tensile strength and Poisson's ratio has been responsible for remarkably planar and extensive sheeting joints, as seen in mountain walls (Barton and Shen, 2018).

Peng et al. (2019) studied the influence of roughness anisotropy on the shear behavior of both shear and tensile joints. They found that compared with other roughness parameters (e.g. average dip angle and fractal dimension), the *JRC* value can be an effective indicator for analyzing roughness anisotropy. Later, Yong et al. (2019) concluded that statistical analysis of the *JRC* might increase the precision and dependability of the roughness estimation results. Bao et al. (2020) studied roughness anisotropy based on 31 natural joint samples. A 3D laser scanning approach was used for digitizing the joint morphology, and the *JRC* values in different orientations were obtained, considering the influences of the sampling interval (*SI*) on the *JRC* calculation process. It was discovered that the *JRC* values exhibited notable anisotropy and substantial variance in particular orientations. In the above studies, there is a consistent conclusion that the roughness of the joint surface has a distinct directionality. In addition to the *JRC*, the 3D directional roughness metric $\theta^*_{\max}/(C+1)_{3D}$ ($\theta^*_{\max}$ is the maximum apparent asperity inclination, and C is an empirical fitting parameter) and corresponding 2D directional roughness metric $\theta^*_{\max}/(C+1)_{2D}$ also reflected obvious roughness anisotropy (Grasselli, 2001; Grasselli et al., 2002; Tatone, 2009; Tatone and Grasselli, 2009, 2010; Magsipoc et al., 2020). Of course, the joints selected for such testing may represent a biased sample with anisotropy obvious to see. However, the polar plots of the *JRC* fail to quantify the roughness variations due to the difficulty in mathematically describing the irregular patterns of *JRC* polar plots.

Yong et al. (2019) suggested a *class ratio transform method* to quantify roughness anisotropy. By doing so, the *JRC*'s directional variability frequently displays a comparatively systematic fluctuation that can be described by the ellipse function with high fitting precision. Du et al. (2021) studied the anisotropy characteristics of rock joint roughness through *JRC* statistical analysis. As shown in Fig. 12a, the frequency histograms of *JRC* values in the same orientation follow normal distributions. The polar plots of the mean *JRC* values in different orientations were applied to represent the roughness anisotropy of the entire joint surface (Fig. 12b). It shows that the results based on statistical analysis also show irregular roughness in different orientations. Therefore, they characterized the anisotropy of joint roughness by local anisotropy and global anisotropy. The local anisotropy indicates the variation between adjacent orientations, and the global anisotropy reflects the difference between major and minor values of *JRC* in various orientations.

5.2. Scale effect

The scale effect impacts the strength and deformability of rock joints. Since the 1970s, the scale dependence of the strength of rock joints has been studied by many researchers (e.g. Barton, 1973; Barton and Choubey, 1977; Bandis, 1980; Bandis et al., 1981; Barton, 1982; Barton et al., 1985; Du and Fan, 1999; Johansson, 2009; Tatone and Grasselli, 2010; Hencher and Richards, 2015; Yong et al., 2017). The main reason behind the generally assumed 'negative' shear strength scale effect (i.e. reduction with size) is that roughness, a key parameter controlling shear strength, is itself scale-dependent. Hence, the variations in the roughness of rock joints with different sizes, including anisotropy, need to be thoroughly considered.

In practice, it is found that the *JRC* is scale-dependent. Usually, longer profiles or larger blocks containing the same joint have lower *JRC* values. Two examples of the scale effects on rock joints are illustrated in Fig. 13. As shown in Fig. 13a, tilt tests were conducted to evaluate the *JRC* values of the larger and smaller samples obtained from the same natural rock joint (Barton and Choubey, 1977). The tilt angle was always 59° for the 45 cm long sample. Then, the large joint sample was sawed into 18 equal samples with a size of 4.8 cm × 9.8 cm. The mean tilt angle of these small samples was 67.2°. Based on the back analysis, the calculated *JRC* value for the large sample was 5.2, but the mean value was 8.8 for the small samples. Fig. 13b shows that smaller blocks have greater freedom to

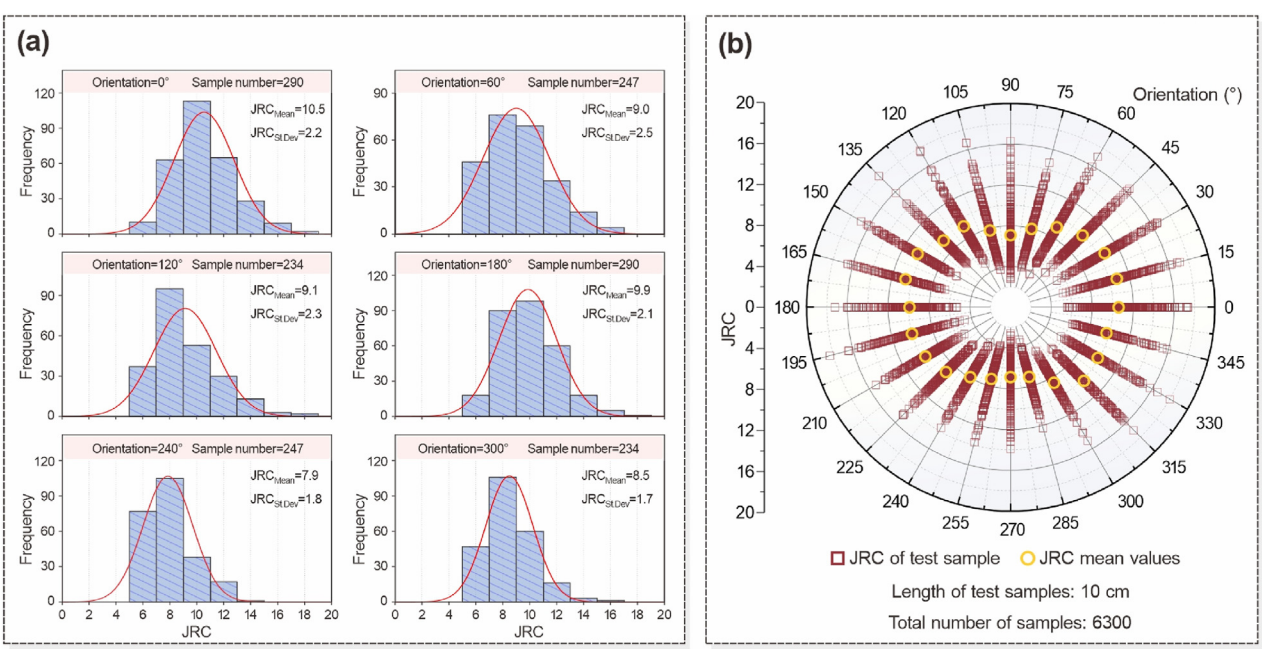

Fig. 12. (a) The frequency histograms of *JRC* values in orientations of 0°, 60°, 120°, 180°, 240° and 300°; and (b) The polar plots of the *JRC* values in steps of 15° from 0° to 360° (after Du et al., 2021).

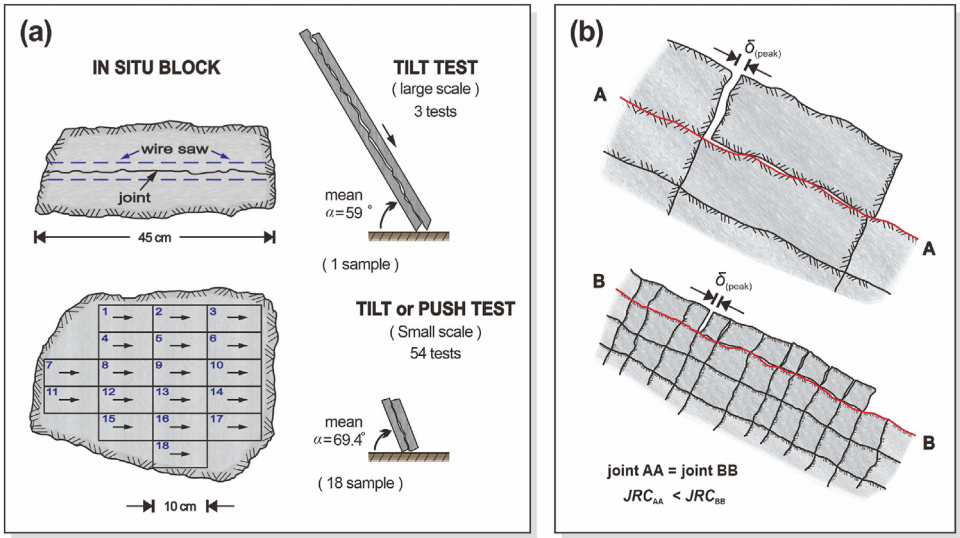

Fig. 13. (a) Scale effect investigation with tilt tests of a 45 cm long joint in granite, followed by individual tilt tests on eighteen component samples from the same joint, sheared in the same direction; and (b) Contrasting *effective JRC* of widely and close spaced joints (after Barton and Choubey, 1977).

follow and 'feel' the smaller scale and steeper asperities of the component joints; hence, higher *JRC* values are evident. Therefore, a joint with small, steep asperities influencing peak behavior would have a greater *JRC* value at small scale than a longer profile of the same joint where larger, less steeply inclined surface features will determine the joint's behavior.

The scale dependence of the *JRC* was also clearly demonstrated by Bandis et al. (1981) through a comprehensive series of shear tests. Based on the results of extensive testing of rock joints, joint replicas, and a comprehensive survey of the literature, Barton and Bandis (1982) presented *JRC*, *JCS* scale correction curves, as shown in Fig. 14, and the following equations for describing the reductions in the *JRC* and *JCS* with increasing sample size were suggested:

$$JRC_n \approx JRC_o (L_n/L_o)^{-0.02JRC_o} \tag{18}$$

$$JCS_n \approx JCS_o (L_n/L_o)^{-0.03JRC_o} \tag{19}$$

where JRC_o and JCS_o refer to the *JRC* and *JCS* when measured in the laboratory with a nominal length of $L_o = 100$ mm (or similar) and JRC_n and JCS_n refer to the *JRC* and *JCS* when extrapolated to the desired length of L_n. The latter is expected to be the relevant block size given by the mean spacing of cross-joints.

Based on the statistical analysis of the *JRC* values of 1157 joint profiles obtained from Xiaolangdi Reservoir Area, Du (1992) developed a similar method for various size-dependent characterizations of joint roughness. The fractal expression of the *JRC* and the sample size is given as follows:

$$JRC_n = JRC_o (L_n/L_o)^{-D_n} \tag{20}$$

where D_n is the fractal dimension of the *JRC* scale effect, which defines the magnitude of the change in JRC_n that decreases as the sample length L_n increases. For the convenience of engineering application of the scale effect laws in Eq. (20), Du and Fan (1999) proposed a method for D_n determination based on its relationship to the back-calculated fractal dimension (D_3) of 300 mm long joint profiles. They summarized the value of JRC_o and D_3 for typical rock joints based on a comprehensive study of 11,064 joint profiles obtained from 16 different rock types.

The joint roughness can be characterized by two components: waviness (large-scale undulation) and unevenness (small-scale roughness). The waviness becomes more dominant with the increasing scale of rock joints, while the significance of the unevenness decreases. Barton and Choubey (1977) suggested that the correct size of the joint for indexing (shear testing or surface analysis) might, as a first approximation, be given by the natural block size (specifically the spacing of cross-joints). This suggestion was reinforced by the biaxial testing of '2D slabs' with 250, 1000 and 4000 tension-fractured blocks by Barton, which was reported in Barton and Hansteen (1979) and in Bandis et al. (1981). This block size study was made using the same model tension fracture techniques Barton had used a decade earlier in his model slope stability studies with 40,000 blocks. Later, some researchers found that the surface roughness becomes statistically stationary when the scale of the rock joint (or block size) reaches a certain value. This size was defined as the stationarity threshold (*ST*) by Jing and Hudson (2004), and it is similar to the definition of representative elementary volume (*REV*) of fractured rock, which allows the establishment of representative geometric parameters for aggregates at fracture surfaces over a wide range. Theoretically, testing results taken using rock joint samples at a scale equivalent to or larger than its *ST* are the only way to accurately determine the mechanical behavior of a rock joint. The results with sample sizes smaller than *ST* cannot be directly applied to representing fracture behavior at field scales. For an accurate determination of the surface roughness of rock joints at a large scale, Yong et al. (2020) suggested a technique for the estimation of *ST* based on *JRC* statistical analysis. They combined the lower/upper limits of *JRC* and the mean values of *JRC* for the joint sample lengths from 100 mm to 3000 mm to investigate the scale effects on joint roughness (Fig. 15a). Based on the derivative of the *JRC* neutrosophic functions, the variation trend of the relationship between *JRC* and the sample size was assessed. As shown in Fig. 15b, the derivative suggested that the *JRC* value for small samples is more sensitive than the *JRC* value for large samples. It is recommended that *ST* can be determined when the derivative value is equal to −0.05 because the

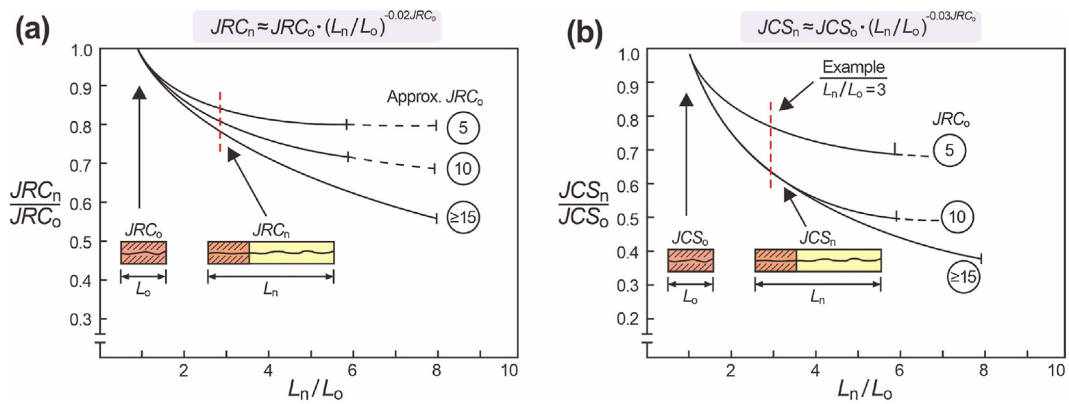

Fig. 14. Scale effect correction for *JRC* and *JCS* (Barton and Bandis, 1982).

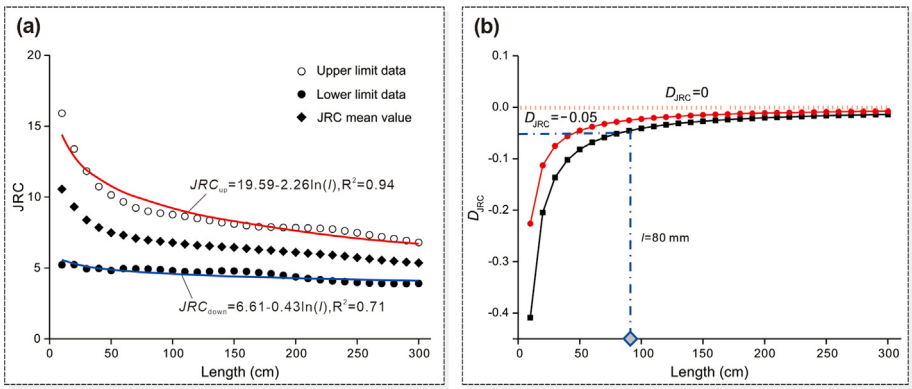

Fig. 15. (a) The lower and upper limits and the mean values of *JRC* of different-sized joint samples, and (b) The ST determination based on the derivative of *JRC neutrosophic* functions (after Yong et al., 2020).

roughness behavior is almost independent of scale when the sample size exceeds the determined value.

5.3. Coupled behavior of anisotropy and scale effect of joint roughness

As we have just seen, surface roughness varies not only with orientation but also with scale. Since the properties of anisotropy and scale effects are not isolated but interrelated, some researchers have systematically studied the coupled behavior of anisotropy and the scale effects of joint roughness. Tatone (2009) studied the dependency of joint roughness on the sizes of sampling windows. He found that the roughness parameters in different orientations appear to converge to a constant value as the sample window size is increased, resulting in a decrease in anisotropy variation. Du et al. (2021) made a statistical analysis on the *JRC* values of 19, 616 different-sized profiles. They found that the mean and standard deviation of the *JRC* in each orientation decreased with increasing profile size, indicating a negative scale effect on joint roughness. According to the variations of *JRC* mean values in each orientation, they found that ST was 600 mm. When the sample size exceeded ST, the global anisotropy tended to remain constant.

Furthermore, heterogeneity, anisotropy, nonuniformity, and inherent scale effects are the characteristics of joint roughness, which naturally brings some uncertainty to the joint roughness measurements (Du and Pan, 1992). Since there is incomplete and indeterminate information in the *JRC* values of different-sized samples at various orientations, it brings difficulties to investigate the coupled behavior of anisotropy and scale effect based on classical probability and statistics. To solve this problem, many researchers (Ye et al., 2017; Chen et al., 2017a, 2017b; Yong et al., 2019; Song et al., 2021) proposed different methods based on neutrosophic theory to express the anisotropy based on the *JRC* data of different-sized rock joints. Using these methods, the fuzzy information of *JRC* is not lost, and the original information of the roughness properties is preserved to the greatest extent. As shown in Fig. 16, the heterogeneity of the surface roughness is described by the *JRC* values, which are indeterminate between the upper and lower bounds, accounting for both the roughness anisotropy and

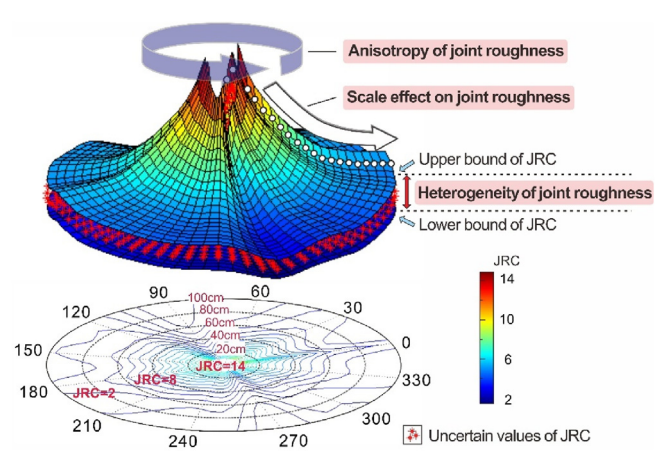

Fig. 16. Roughness characteristic description based on *JRC*.

the scale effect. Many excellent research groups did productive works on the *JRC* and rock joint shear strength, such as Barton et al. (Barton, 1973, 1982, 1990, 2013, 2020; Barton and Choubey, 1977; Barton and Bandis, 1982, 2017; Barton et al., 1985; Barton and Quadros, 1997, 2015, 2019), Fardin et al. (Fardin et al., 2001, 2004; Fardin, 2008), Kulatilake et al. (Kulatilake et al., 2006, 2021; Ge et al., 2014), Grasselli et al. (Grasselli, 2001; Grasselli et al., 2002; Grasselli and Egger, 2003; Tatone and Grasselli, 2009, 2010; Magsipoc et al., 2020), Du et al. (Ye et al., 2016, 2017; Yong et al., 2017, 2018a, 2018b, 2019, 2020), Zhu et al. (Chen et al., 2015; Liu et al., 2021, 2022), Liu et al. (Liu et al., 2017a, 2017b, b; Tian et al., 2018a, 2018b), and many others. Amongst the research groups worldwide, significant contributions have now been made to the topic of rock joint shear strength over the years. An example is the highly-acclaimed expert in China, Professor Shigui Du and his research group, who have made significant efforts and achievements in the theory, equipment, technology and engineering application of rock mass in terms of shear strength of sliding surfaces. They also realized an accurate acquisition of shear strength. It is exciting that Du's research team has been becoming one of the promising academic research centers in rock mechanics in terms of *JRC* and shear strength across the world.

6. Descriptions of properties of rock joints based on the *JRC*

Realistic characterization of the mechanical and hydraulic properties of rock joints has been an important goal of rock mass engineering for many years. Even simplified constitutive models demonstrate the extreme importance of joint characteristics. For example, a simple change in the friction angle from 40° to 30° may alter not only the magnitudes of deformation but also the type of deformation experienced by an excavation. In this section, we focus on the descriptions of the properties of rock joints based on the *JRC*. Other roughness parameters, such as fractal dimensions and statistical parameters that can potentially characterize the mechanical and hydraulic properties of rock joints exist (e.g. Goodman, 1974; Jing et al., 1992; Grasselli and Egger, 2003; Buzzi and Casagrande, 2018; Kulatilake et al., 2021) but are not discussed here.

6.1. Shear stress-displacement behavior

The shear behavior of rock joints is extremely significant in stability and deformation analyses of rock masses. The *JRC-JCS* model can be conveniently applied in engineering practice based on some simple index tests. This empirical model was complemented by a joint match coefficient (*JMC*) proposed by Zhao (1997). These models initially considered just peak shear strength, and the *JRC* introduced up to now is particularly correlated to the peak shear strength of rock joints. The peak shear strength of a rock join is actually mobilized by a small shear displacement (δ_{peak}). As indicated by Barton and Bandis (1982), δ_{peak} is approximately 1% of the length (L) of laboratory-scale samples (approximately 100 mm). However, δ_{peak} may be less than $0.01L$ for joints with lengths of several meters. It is found that the ratio δ_{peak}/L is correlated to the *JRC* and length of a rock joint (Bandis et al., 1981). Based on the data provided by Bandis et al. (1981), Barton (1982) proposed the following equation to estimate the δ_{peak}:

$$\delta_{peak} = \frac{L}{500}\left(\frac{JRC}{L}\right)^{0.33} \tag{21}$$

During the shear displacement before δ_{peak}, roughness and friction both mobilize initially, leading to dilation. Post-peak, roughness is gradually removed or worn away at displacements greater than δ_{peak}. After the peak, dilation continues at a slower rate. At any given shear displacement (δ), the strength is simply represented by the mobilized shear strength (τ_m), whose value is dependent on the magnitude of $JRC_{mobilized}$:

$$\tau_m = \sigma_n \tan\left[JRC_{mobilized} \log_{10}\left(\frac{JCS}{\sigma_n}\right) + \varphi_r\right] \tag{22}$$

Barton (1982) demonstrated that the dimensionless coordinates $JRC_{mobilized}/JRC_{peak}$ and δ/δ_{peak} grow and then decline essentially identically during shear for a wide variety of joint surfaces and stress levels. Fig. 17 depicts examples of the behavior of shear stress versus displacement. The simplified table for non-planar joints, given as an insert in Fig. 17, provides the essential coordinates for defining a full shear stress-displacement (and dilation) event. The resulting curves might vary from highly pointed to smooth and rounded, as seen when larger block sizes are modeled.

There are many other approaches describing the behavior of shear stress-displacement for rock joints, including three main categories: theoretical, empirical, and numerical simulation methods. To mimic the observed shear behavior of rock joints, the theoretical method employs established theories such as plasticity theory, contact theory, energy theory, adhesion theory, wear theory, and fractal geometry. In the empirical approach, empirical models are formulated by analyzing physical data obtained from test results and deriving correlations using variables of influence (as in Fig. 17). The numerical simulation approach mainly adopts the discrete element method (DEM) or the finite element method (FEM) to simulate the shear behavior of rock joints. These methods for characterizing the shear behavior of rock joints aid scientists in comprehending the fundamental mechanical features of rock joints under shear.

6.2. Dilation behavior

When a nonplanar joint is sheared, the opposing asperities slide across each other, resulting in an increase in aperture. This dilation process begins with a limited displacement and progresses with an accelerating gradient as peak strength is approached. The dilation behavior has a considerable impact on the shear strength of rock joints. Goodman (1970), Barton (1973), and Pratt et al. (1974) have verified that peak dilation is reached at or shortly after peak shear strength, thus demonstrating a significant link between dilatancy and the peak shear strength of rock joints.

On the basis of the direct shear test findings of 136 specimens, Barton and Choubey (1977) examined the connection between the asperity component of peak strength and dilation angle. The asperity component is equal to the difference between the total friction angle measured ($\arctan(\tau/\sigma_n)$) and the residual friction angle estimated (φ_r). The peak dilation angle (d_n) and the initial dilation angle (d_i) are shown plotted against the asperity component in Fig. 18. The mean value of the *initial* dilation angle (d_i) is approximately one-third of the asperity component, as seen in the graph:

$$d_i = JRC \log_{10}(JCS / \sigma_n) / 3 \tag{23}$$

while the majority of *peak* dilation angles (d_n) fell between the following limits:

$$JRC \log_{10}(JCS / \sigma_n) / 2 < d_n < 2JRC \log_{10}(JCS / \sigma_n) \tag{24}$$

The value of d_n changes with the applied normal stress level, the *JRC*, and the *JCS*. Where asperity damage is minimal (as a result of relatively high *JCS* values, low σ_n values, or small *JRC* values), the asperity component $JRC \log_{10}(JCS/\sigma_n)$ provides the best

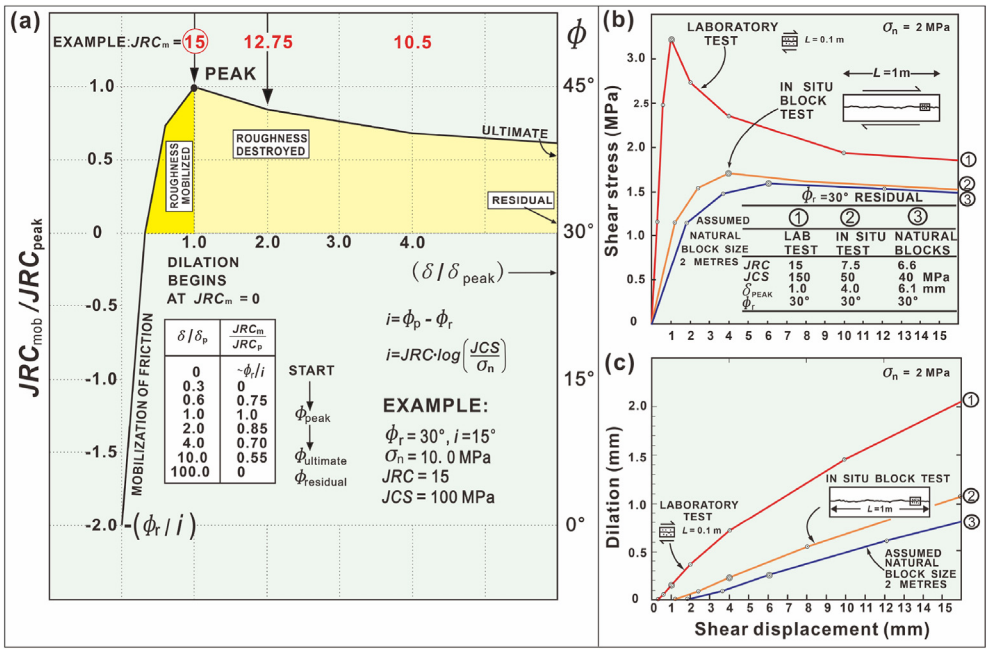

Fig. 17. (a) Model suggested for producing realistic shear stress-displacement curves for non-planar joints, and (b, c) Examples of stress-displacement-dilation modeling with scale effect assumptions (Eq. (18) and (19)) given in the inset (after Barton, 1982).

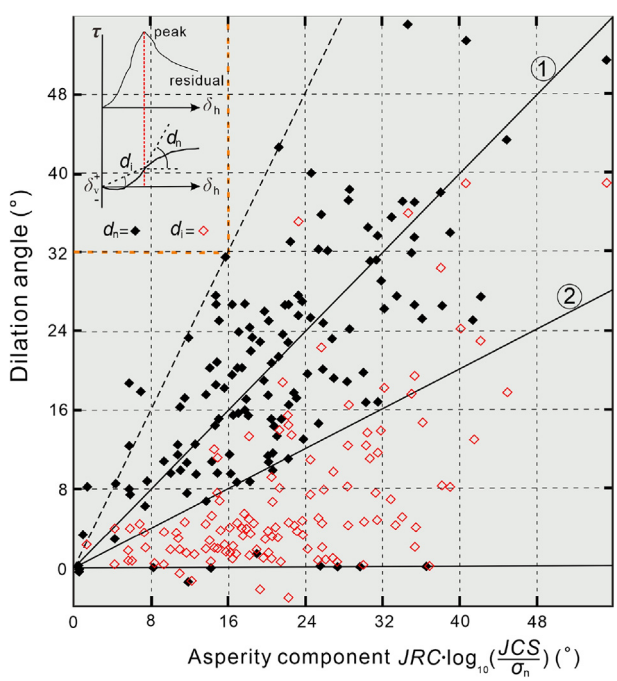

Fig. 18. Distribution of peak and initial dilation angles and their relationship with the asperity component of shear strength (after Barton and Choubey, 1977).

approximation of the d_n. As seen in Fig. 18, the middle envelope (line 1) is a near approximation of the mean performance of the 136 tested rock joint samples, though there is wide scatter. In contrast, the asperity component estimate of *JRC* $\log_{10}(JCS/\sigma_n)/2$ provides a more accurate estimation of the d_n for the 130 tests on tension fractures in model materials published by Barton (1971), in which the tests were conducted at normal stress levels that resulted in significantly greater asperity damage than that observed in Fig. 18. Based on these observations and analysis, Barton and Choubey (1977) defined a joint damage coefficient (M) to correlate the peak friction angle and asperity components:

$$M = \frac{JRC}{d_n}\log_{10}(JCS/\sigma_n) \tag{25}$$

Shearing at low or high normal stress, respectively, results in a damage coefficient (M) of 1 or 2 (Olsson and Barton, 2001). Alternatively, it may be approximated by the formula below (Barton and Choubey, 1977):

$$M = \frac{JRC}{12\log_{10}(JCS/\sigma_n)} + 0.7 \tag{26}$$

Based on the appropriately selected damage coefficient (M) and mobilized *JRC* values, the dilation-shear displacement behavior can be quantitatively obtained. For example, Xia et al. (2014) adopted Eq. (27) to estimate the peak joint dilatancy angle for their test results by assuming that the damage coefficient (M) equals 1 and proposed a peak dilatancy angle function using the roughness parameters derived by Grasselli et al. (2003). Notably, the value of δ/δ_{peak} at which dilation is supposed to begin is 0.3, both for nonplanar and planar joints (Barton, 1982).

6.3. Joint closure behavior

For the study of the mechanical/hydromechanical behavior of rock masses, the closure behavior of rock joints under normal loads is of essential interest. It should be noted that the closure behavior of rock joints with or without filled materials is significantly different. For the filled joints, the closure behavior of rock joints mainly depends on the properties of filled materials, the degree of filling, and the roughness of joints (Ladanyi and Archambault, 1977; Huang et al., 2018; Tian et al., 2018b). In this section, we mainly focus on the closure behavior of unfilled rock joints. Bandis (1980) found that the maximum closure (V_m) of joints with a comparable average value of initial aperture (a_j) was predominantly determined by the *JCS*. Variations in the V_m of joints with comparable *JCS* and

aperture values were correlated with the *JRC*. Large values for the maximum closure were recorded for certain weathered joints, due to the combined impact of greater initial apertures and low *JCS* values. The ratio JCS/a_j was found to be a sensitive indicator of this behavior; low ratios give large values of V_m and vice versa. An analysis of the experimental data reported by Bandis (1980) showed that the following simplified empirical relation gives a reasonable estimate of the initial unstressed aperture of a joint (Barton, 1982):

$$a_j = \frac{JRC}{5}\left(0.2\frac{\sigma_c}{JCS} - 0.1\right) \tag{27}$$

where a_j is the initial joint aperture expressed in mm under self-weight stress (approximately 0.001 MPa), and σ_c is the unconfined compressive strength of the intact rock. Bandis (1980) fit a wide range of experimental data for maximum closure, with the following empirical relationship:

$$V_m = A + BJRC + C\left(\frac{JCS}{a_j}\right)^D \tag{28}$$

where *A*, *B*, *C*, and *D* are the constants obtained from experimental data. Notably, Eq. (28) is a simple constitutive equation that presents the differences in the maximum closure of unfilled interlocked joint types with the following range of wall strength and geometry indices, i.e. $JRC = 5–15$, $JCS = 22–182$ MPa, and $a_j = 0.1–0.6$ mm, the latter assuming that the initial stress condition does not exceed a level of approximately 0.001 MPa (i.e. essentially unstressed). Due to the nonlinear relationship between the closure deformation of the rock joint and the normal stress, Goodman (1974) proposed two hyperbolic functions to describe joint closure under normal stress, whereas Bandis (1980) derived a single hyperbolic model to describe the aperture deformation of a rock joint under normal stress. This hyperbolic model was shown to give an improved fit to experimental data when compared to the two hyperbolic functions suggested by Goodman (1974). It is expressed as follows:

$$\sigma_n = \frac{\Delta V_j}{a - b\Delta V_j} \tag{29}$$

where *a* and *b* are the constants and ΔV_j is the joint closure. Note that the asymptote of the hyperbola (a/b) equals the maximum joint closure (V_m), and that the constant *a* equals the reciprocal of the initial normal stiffness (K_{ni}). Simplifying from Bandis (1980), Barton (1982) suggested that the initial normal stiffness (K_{ni}) could be estimated by the following relationship:

$$K_{ni} = 0.02(JCS / a_j) + 2JRC - 10 \tag{30}$$

Expressions for K_{ni} and V_m therefore define the complete stress-closure behavior of rock joints. Then, for each increase of σ_n, the appropriate K_n value may be calculated using the Bandis (1980) hyperbolic function derivative:

$$K_n = K_{ni}\left(1 - \frac{\sigma_n}{V_m K_{ni} + \sigma_n}\right)^{-2} \tag{31}$$

There have been several additional models created to represent the mechanical behavior of a joint under normal stress. There are three classifications for these models: empirical, theoretical and numerical. Empirical models are employed to fit experimental data with simple nonlinear mathematical functions (Swan, 1983; Malama and Kulatilake, 2003). Under normal load, theoretical models based on the Hertz contact theory may be utilized to estimate the closure deformation of joints (Greenwood and Williamson, 1966; Greenwood and Tripp, 1970; Brown and Scholz, 1985). Multiple numerical models with asperities simulated by cylinders can account for both asperity deformations and rock deformations around the asperities (Cook, 1992; Lee and Harrison, 2001; Marache et al., 2008).

Considering the differences of influences between the waviness and unevenness components on the closure deformation, Xia et al. (2003) determined the impacts of the waviness and unevenness components based on a mathematical method and proposed a generic load-closure model. Based on the Xia et al. (2003) model, Tang et al. (2013) presented an improved model considering the deformation produced by asperity deformation and the interaction between asperities. Perhaps with some similarity to the latter, Barton (2020) recently suggested that *over-closure* and *thermal over-closure* of rock joints, in which actual tensile strength is developed in the case of moderately-rough and rough rock joints, may be caused by the 'perpendicular' '*JRC*' involving the friction between interlocking and sloping asperities. He suggested this has caused some of the reported difficulties with geothermal projects in which 'cold' injected water is 'captured' by joint sets with lower *JRC* since they will not be over-closed so can open due to the shrinkage/cooling and conduct water away from the 'producer' well, since shearing more readily as a result of their smoother character.

6.4. Conductivity of rock joints

Variations in the hydraulic conductivity of rock joints resulting from changes in normal or shear stresses are closely related to some engineering geological disasters at dam sites. The potential leakage of reservoirs, the leakage of contaminated radioactive water, the instability of dam foundations, slopes, and underground caverns, and the extraction of oil and gas are each related to the conductivity of rock joints and how this varies with changes of effective normal stress and eventual shearing and dilation. It is not possible to adequately predict the mechanical and hydraulic behavior of rock joints when exposed to a change in stress, unless an accurate method can be derived for measuring real joint apertures in situ prior to a stress perturbation. The unknown stress history of joints in situ means that the techniques developed in Section 6.3 only provide a crude approximation to apertures in situ, even if the present stress distribution is known.

Experiments in the laboratory have shown that the aperture and the roughness of a rock joint are the two most essential factors influencing fluid flow through the joint.

When modeling the influence of joint conductivity, at least two types of joint apertures must be considered: the mean physical aperture (*E*) and the (theoretical) hydraulic aperture (*e*) (Barton, 1972; Barton, 1982; Barton et al., 1985; Barton and Quadros, 1997; Olsson and Barton, 2001; and subsequently many other authors). The real physical aperture (*E*) is larger than the conducting aperture (*e*) for rough joints. How to link the hydraulic apertures (*e*) to the normally larger mean physical apertures (*E*) is thus a crucial topic. (Note that the mean physical aperture *E* incorporates the 'reducing-of-the-mean' effect of asperities/surfaces in local contact if and when transmitting positive effective normal stresses.)

Fig. 19 displays test data from which apertures *e* and *E* (or Δe and ΔE) were measured (Barton et al., 1985, updated by Quadros in Barton and Quadros, 1997), demonstrating that as the aperture lowers, the divergence between *e* and *E* (or Δe and ΔE) increases. The bars marked NS, EW and B represent large-scale block test data from Hardin et al. (1982) and indicate whether there was a shear stress component (NS or EW) or whether stresses were biaxial (B) resulting in pure normal stress across the test joint. It is apparent that the cubic law with $E = e$, may only be valid when joints are

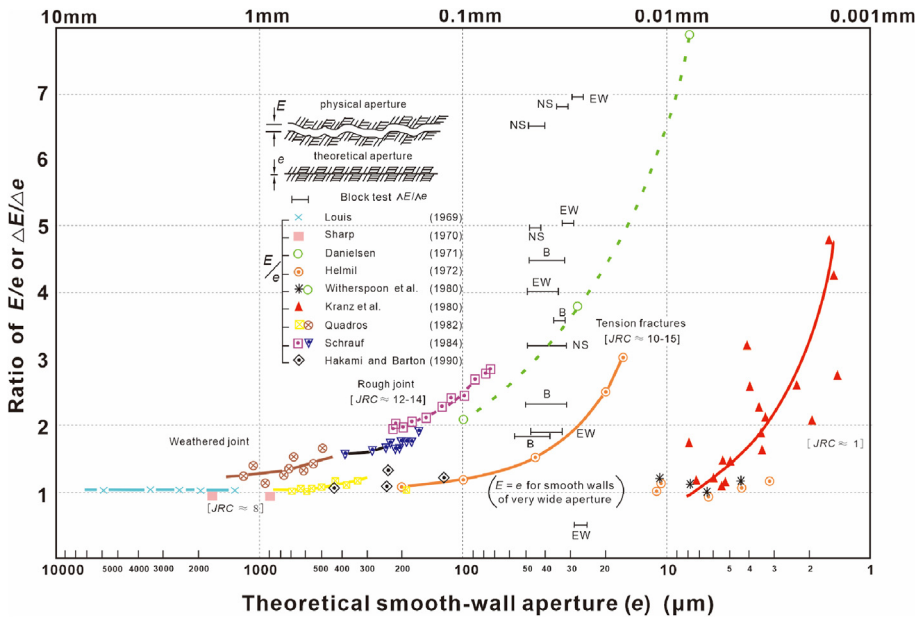

Fig. 19. Relationship between the ratio of mean physical aperture and the theoretical hydraulic aperture in terms of *JRC, based on the parallel-plate flow analogy* (after Barton and Quadros, 1997).

exceptionally smooth, or when apertures are very wide. These observations of the dependence of E/e on the joint roughness and aperture lead to the formulation proposed in Fig. 20. It can be seen that bias from the cubic equation ($E = e$) is modeled for rough joints of very wide aperture ($\geq$1 mm). No divergence is modeled for the smoothest joints unless hydraulic apertures are very small (i.e. $<$10 μm). These features of the model broadly correspond with observed behavior. It also determines the types of contacts, and therefore indirectly the tortuosity of flow and the frictional drag resisting flow between joint walls. The following equation (Barton, 1982) represents the curve in Fig. 20:

$$e = \frac{JRC^{2.5}}{(E/e)^2} \tag{32}$$

where E and e are expressed in μm. An alternative form of this equation is given below:

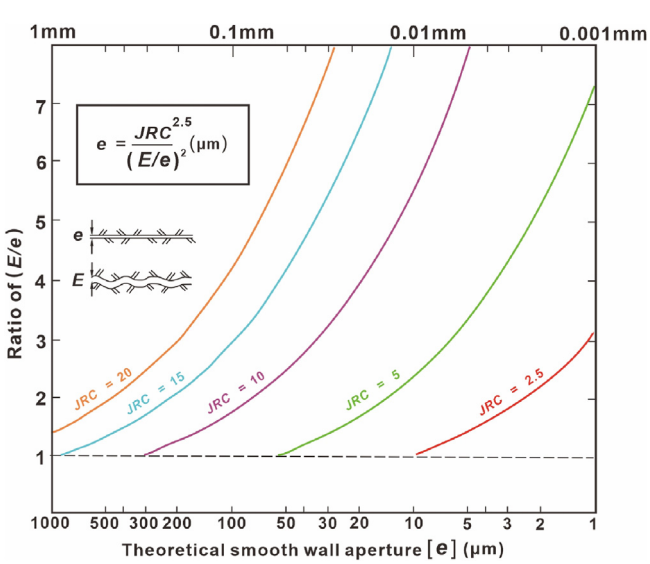

Fig. 20. A constitutive model relating hydraulic aperture with physical aperture and joint roughness (Barton, 1982).

$$e = E^2 \big/ JRC^{2.5} \tag{33}$$

Eqs. (32) and (33) are only applicable for values of $E/e \geq 1$ with modest shear displacement and insignificant gouge generation. The joint closure is unlikely to be size-dependent, unlike the shear stress-displacement behavior, hence these equations enable one to link E and e even at the field scale (Barton, 1982; Barton and Quadros, 1997, 2019). The above aperture equations are approximate (Barton, 2020), but the formulae have been widely applied to converting hydraulically measured e into E at field scale for various geoengineering problems (Barton, 1972, 1982; Bandis et al., 1985; Barton and Bakhtar, 1987; Bhasin et al., 2002; Ishii, 2020) including for assisting in the choice of grout particle sizes using the $E > 4d_{95}$ rule of thumb. This is apparently not used in Swedish pre-grouting of tunnels, where the theoretical hydraulic e-aperture is (surprisingly) used for estimating grout entry.

7. Influences of the *JRC* on the properties of rock masses

Probably several million structures and constructions such as slopes, tunnels, and dams are distributed in a multitude of jointed and fractured rock masses, and these inevitably have almost worldwide locations. The properties of rock masses, including strength, deformation, and quality, are closely related to the properties of rock joints. Additionally, some interfaces such as rock-soil, concrete-rock, and clay-concrete also have significant influences on the properties of both natural and bolted rock masses. Engineering procedures commonly include bolted rock masses because it is the most efficient and cost-effective way to support excavations in rock masses. In this section, we focus on the influences of *JRC* on the properties of natural rock masses, bolted rock masses, and some frequently encountered interfaces.

7.1. Natural rock masses

The characteristics of rock joints have a significant impact on the strength and deformability of rock masses. Barton and Bandis (1982) emphasized that the block size significantly affects the

shear strength of jointed rocks. As shown in Fig. 21, for an unchanged *JRC*, the shear strength of an assembly of blocks decreases with increasing block size. The biaxial shear tests shown in the figure were reported by Barton and Hansteen (1979) using the tension-fractured brittle model materials and the double-bladed guillotine to generate intersecting sets of equally spaced fractures, as used by Barton (1971). The experiments were conducted prior to large-span cavern modeling (for underground nuclear power plant uses), employing a variety of fracture configurations provided by 20,000 blocks and low and high horizontal stress levels. The tests were pre-UDEC and hence pre-UDEC-BB. Depending on the joint spacing used, each of the considerably smaller biaxial models was made up of 4000, 1000 or 250 blocks. In every instance, the joint orientation ($2\beta = 36°$) and loading route (constant σ_2, rising σ_1 until failure) were the same. The additional freedom for block rotation in the case of the smallest-block models caused higher shear strength and allowed kink-band development. Nevertheless, the models with smaller blocks showed lower deformation moduli as expected. Shear box samples (length L_4) in these physical model investigations may be longer than block size dimensions L_1, L_2 or L_3, so may underestimate the jointed rock mass's shear strength. By comparison, shear box samples are typically smaller than even L_1 in the practice of rock mechanics and, unless scale-corrected, frequently overestimate the shear strength of the rock mass.

The characterization of rock joint properties has long been recognized as an important process in describing the properties of rock masses. This of course has been the reason for rock mass descriptive schemes like the *Q*-system with its several joint-related parameters. It will be discussed later. Since rock mass behavior is frequently dominated by joint behavior as opposed to modified intact rock curve fitting, Barton (1999) proposed easily understood empirical equations designed to symbolically represent the *progressively mobilized* strength components of fractured and jointed rock, as assembled in Fig. 22. Recently Barton (2021) 'christened' these components CcSs (crack, crunch, scrape, swoosh) to represent the successive breakage of intact bridges, shearing on these new rough surfaces, mobilization of joint set responses, and finally engagement of any faults or major clay-filled discontinuities – in other words, the commonly experienced progressive failure and not the usually incorrect addition as in Mohr-Coulomb and Hoek-Brown of '$c + \sigma_n \tan \varphi$' (linear or nonlinear: both will usually be incorrect).

7.2. Rock mass classification

Prior to any excavation or rock disturbance, rock mass classification is one of the most effective techniques in rock mechanics and a crucial component of feasibility assessments. To provide a quantitative indicator of rock mass quality and as guides for engineering design, certain rock mass classification systems, such as the rock mass rating RMR (Bieniawski, 1973), the rock mass quality *Q*-system (Barton et al. 1974), and the simplistic geological strength index GSI (Hoek, 1994), have been widely employed. Based partly on Norwegian and Swedish tunnel and cavern case records published by Cecil (1970), Barton et al. (1974) proposed the empirical rock mass classification system, i.e. the *Q*-system for the evaluation of rock mass characteristics and tunnel support requirements. The *RQD* index, the number of joint sets, the roughness of the weakest joints, the degree of modification or filling along the weakest joints, and two additional parameters that take into consideration the rock load and water inflow, are all factors that affect the rock mass quality *Q*. The appropriate permanent support for the whole range of rock qualities may be estimated using the *Q* values, which range from 0.001 (for exceedingly low quality squeezing ground) to 1000 (for exceptionally good quality rock that is nearly unjointed). The following is a combination of the six inputs used to define the quality of the rock mass:

$$Q = \frac{RQD}{J_n} \frac{J_r}{J_a} \frac{J_w}{SRF} \tag{34}$$

where *RQD* is the rock quality designation (Deere, 1963), J_n is the joint set number, J_r is the joint roughness number, J_a is the joint alteration number, J_w is the joint water reduction factor, and *SRF* is the stress reduction factor. RQD/J_n is a pair of characteristics that serves as a rough gauge for relative block size, J_r/J_a approximately represents the inter-block shear strength, and J_w/SRF may be used to describe the active stress. When there are sufficient joint sets to define blocks, together with the presence of excavation for stress release, the roughness of the principal joint sets will play an important role in determining whether overbreak occurs. It is of interest to note that J_r has been approximately related to *JRC* and to different scales of *JRC* as shown in Fig. 23.

After analyzing the data with the *Q*-system application at the Yellow River Xiaolangdi dam site and with the substantial in situ testing performed by the Yellow River Water and Hydroelectric Power Development Corporation (YRCC, NWR), Barton (1991) discovered that the *Q* value may also be roughly inferred from seismic velocity observations using the following equation in a wide range of rock characteristics:

$$Q = 10^{\frac{V_p - 3500}{1000}} \tag{35}$$

where V_p is the P-wave velocity (m/s). For velocities exceeding 3600 m/s, the following relation may be used to produce an even better fit for fair to good quality granite and gneiss (Barton, 1991):

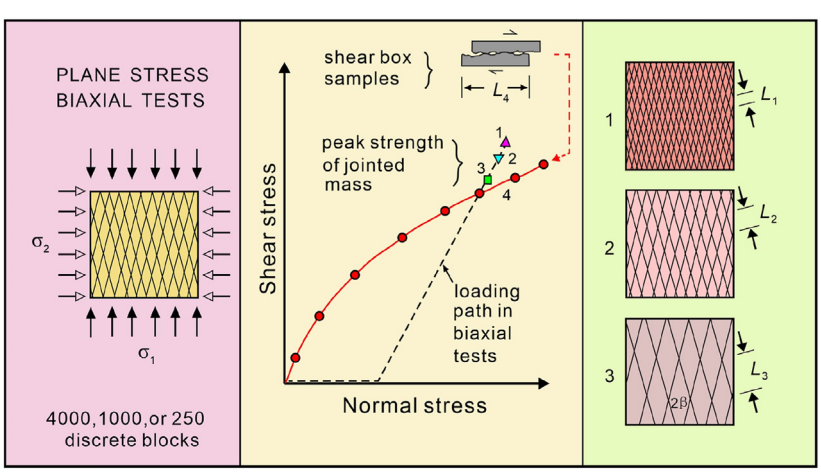

Fig. 21. Shear strength scale effect due to block size (after Barton and Hansteen, 1979 and Bandis et al., 1981. For further experimental details, see Barton and Bandis, 1982).

Please cite this article as: Barton N et al., Advances in joint roughness coefficient (*JRC*) and its engineering applications, Journal of Rock Mechanics and Geotechnical Engineering, https://doi.org/10.1016/j.jrmge.2023.02.002

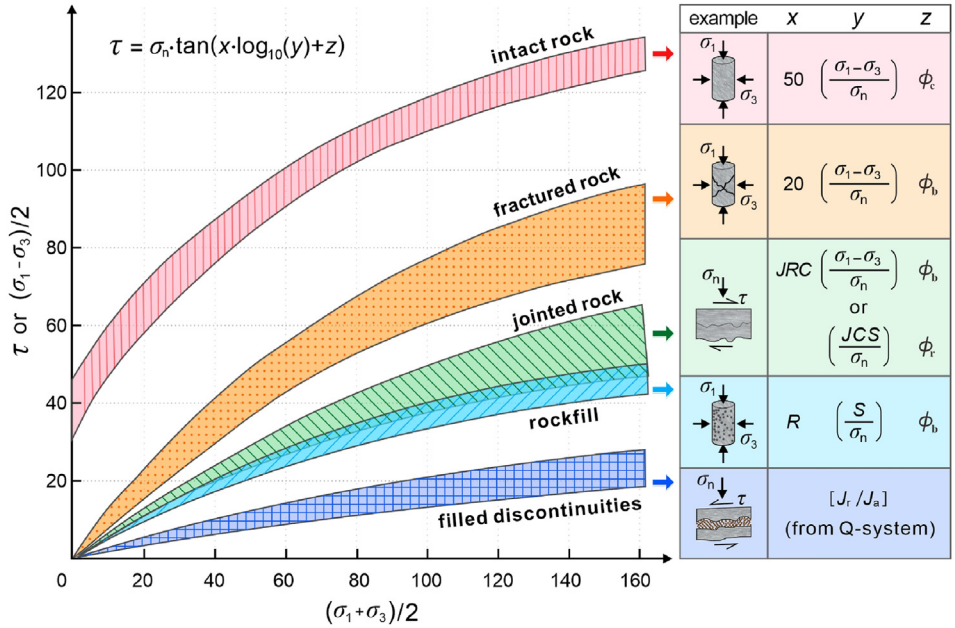

Fig. 22. Principal components of rock mass shear strength (intact, fractured, jointed, filled discontinuities) assembled by Barton (1999). Four of these five shear strength components have recently (Barton, 2021) been adopted in a progressive failure concept termed CcSs representing the breakage of cohesion ('crack'), shearing along these new surfaces ('crunch'), shearing along kinematically capable rock joints ('scrape'), and possible shearing along clay-filled discontinuities of faults ('swoosh'). The components can be quantified using the *x*, *y*, *z* symbols shown in the inset.

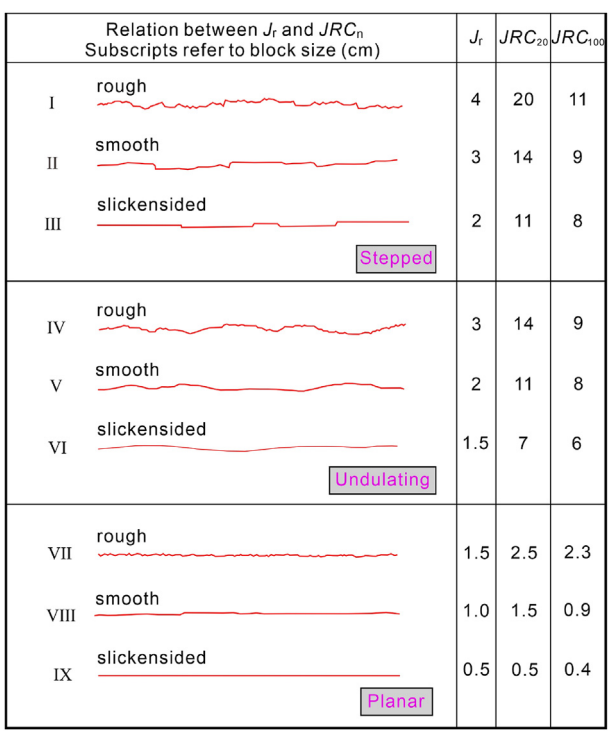

Fig. 23. Correlation between the joint roughness number J_r and *JRC*. The JRC_{20} and JRC_{100} values were illustrative estimates of the possible scale effect encountered with 20 cm and 100 cm block sizes. The J_r ratings are from the *Q*-system (Barton, 1987).

$$Q = \frac{V_p - 3600}{50} \tag{36}$$

Subsequently, Barton (2002) utilized further P-wave velocity data from numerous engineering (and nuclear waste research) sites where *Q*-logging was also performed and presented the depth-dependent correlations between *Q* and V_p shown in Fig. 24. Deep cross-hole velocity measurements were available from the Sellafield site where NGI logged 11 km of core. Note the +ve correction for depth and the -ve correction for the estimated porosity. Further details are given in the textbook on the seismic attributes of rock masses at many scales (Barton, 2006).

Engineering geologists and mining engineers frequently utilize the *Q*-system to characterize rock exposures and drill-cores and to estimate the single-shell support and reinforcement (shotcrete and bolting) required for tunnels, caverns, and mine roadways. Recently, Barton and Bar (2015) presented the *Q*-slope method, a slightly modified *Q*-system for use in benches in opencast mines, motorway cuttings, and road cuttings that are without reinforcement. With the aid of *Q*-slope, engineering geologists, rock engineers, and mining engineers are able to quickly determine the safe unreinforced slope angles of excavated rock slopes in the field and make the best adjustments to slope angles as rock mass conditions become apparent during the construction of road cuts or benches. The following is the formula for calculating the *Q*-slope (note that J_r/J_a can be applied to both sides of potential wedge failures and has orientation weightings):

$$Q_{slope} = \frac{RQD}{J_n}\left(\frac{J_r}{J_a}\right)_0 \frac{J_{wice}}{SRF_{slope}} \tag{37}$$

where the subscript in the parameter pair J_r/J_a is the discontinuity orientation factor, J_{wice} is the environmental and geological condition number, and SRF_{slope} is the rock slope-relevant strength reduction factor. As can be observed in Eq. (38), shear strength input is comparable to that of the *Q*-system but more crucial since wedges are unconfined. In contrast to dilatation around tunnels, shearing typically does not result in an increase in normal stress or stiffness. The same 'contact' strategy applies to filled discontinuities as it did before: (1) rock-to-rock contact, (2) rock-to-rock contact following some shear displacement, and (3) no rock-to-rock contact

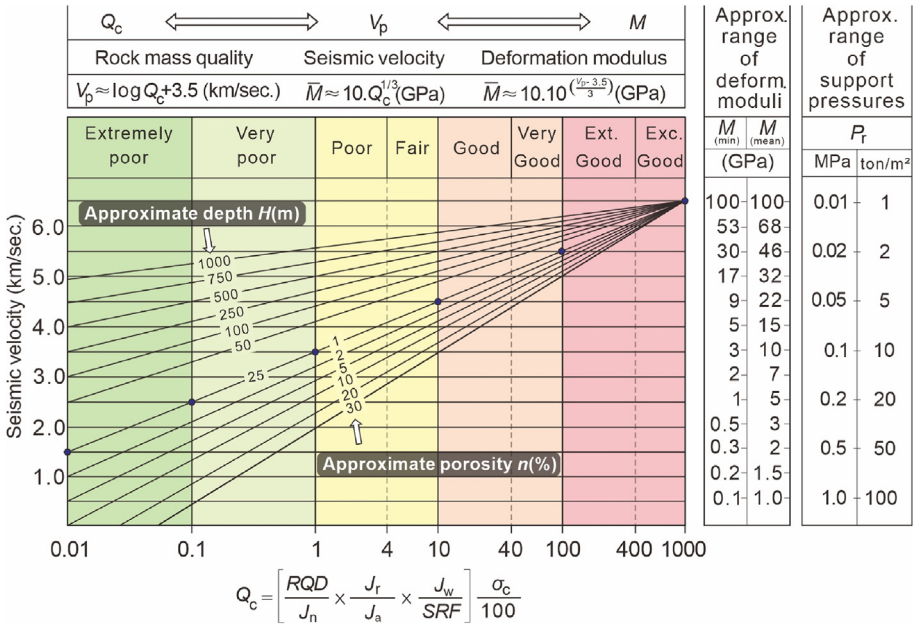

Fig. 24. Approximate empirical correlations between Q_c and V_p with depth correction and links to rock mass deformation moduli and tunnel support pressure needs (Barton, 2002, 2006).

as a result of thick clay fills. The straightforward formula for the steepest safe slope angle (β) without the need for support or reinforcement is

$$\beta = 20 \log_{10} Q_{slope} + 65^\circ \tag{38}$$

Notably, *Q*-slope is suited for application with individual benches in open cast mines, and in road or rail cuttings, or for reinforcement-free site access road cuts. It is not meant to evaluate the stability of high slopes created by many excavation phases over protracted periods of time, such as inter-ramp or overall slopes in open cast mines.

7.3. Bolted rock masses

One of the most efficient and cost-effective methods of reinforcing excavations in rock is rock bolting. To date, the mechanism of bolt implantation into rock masses has been extensively studied under the conditions of pull-out and shear (Bjurström, 1974; Barton and Bakhtar, 1983; Li, 2021).

Since the roughness of rock joints significantly affects the mechanical properties of rock masses, the influence of joint roughness should not be ignored when analyzing bolted rock masses. Some researchers studied the influences of the *JRC* on the shear strength and failure mechanisms of bolted rock joints (Chen et al., 2018; Zhao et al., 2019). In addition to the joint roughness, the installation angle of bolts has an important impact on the shear strength of bolted joints. Bjurström (1974) performed shear tests on 450 mm long jointed blocks and analyzed the influences of the installation angles of the bolts on the shear strength of the bolted joints. Barton and Bakhtar (1983) analyzed the large-scale shear test results and verified optimum installation angles via force diagrams. The laboratory results showed that peak values of shear strength were developed when a grouted bolt was installed at an angle of approximately 35°–50° to the plane of the joint, representing combined shear and tension, consistent with the theoretical force diagrams (Barton and Bakhtar, 1983). Similar results were also obtained by the experimental results from other researchers (Ludvig, 1983; Maiolino and Pellet, 2015).

As discussed above, the rock joint roughness is a crucial factor related to the properties of natural and bolted rock masses. In addition to the joints widespread in engineering rock masses, some interfaces, such as rock-soil, concrete-rock, clay-concrete, and some other interfaces, may be encountered and have significant influences on the properties of both natural and bolted rock masses. Similar to the rock joints, the roughness has long been recognized as a crucial source in evaluating the mechanical properties of interfaces inevitably encountered in engineering practices. For example, the *JRC* has been successfully adopted to investigate the following: the strength and stiffness of the cemented shotcrete-rock interfaces (Saiang et al., 2005), the residual strength of coal–rock interfaces (Li et al., 2015), the bonding or shear strength of concrete–rock interfaces (Mouzannar et al., 2017; Zoorabadi and Carter, 2022), and the time-dependent mechanical properties of the clay–concrete interfaces (Yang et al., 2021).

8. Rock engineering applications

8.1. Continuum or discontinuum?

Rock masses may range from almost intact, through well jointed, to heavily crushed, due to increased proximity to fault zones. The result is variable geometrical patterns resulting from several types of joint sets with their variable roughness and continuity. Notwithstanding an implied need for engineering rationalization, the assessment of strength for such complex media as rock masses cannot be approached based on a single generic strength criterion.

The type, frequency and orientation of the jointing and faulting define the likely modes of deformation, and some indication of the likely ultimate failure mechanism. In significant volumes of rock, there may be two or three classes of discontinuities (natural and stress-induced fracturing) which can become involved in the pre-peak and post-peak deformation and failure. Rock mechanics practitioners to date have generally adopted one of the following

two approaches for the characterization and engineering study of jointed rock:

(1) *A discontinuum approach*, in which the assumed geologic structure is simply but explicitly represented and in turn controls the modes of deformation and mechanisms of ultimate failure (prior to modeling with appropriate rock mass reinforcement).
(2) *A continuum approach*, which involves a semi-empirical simulation of the rock mass, transforming the in situ (actual, assumed) discontinuous state into a hypothetical continuous medium, in which the weakening and softening influence of jointing is supposedly allowed for implicitly.

Due to the complexity, we must resort to numerical UDEC-BB or 3DEC simulations in the case of the discontinuum approach. A useful starting point, and a demonstration of the fundamental differences between M − C and B-B can be gained by performing simulations of large-scale biaxial and triaxial tests. These give a useful insight into mechanisms at failure, and comparisons of shear strength estimates based on the nonlinear BB strength criteria, with linear Mohr-Coulomb (MC) criteria, are quite revealing. Fig. 25 shows that due to the nonlinearity of BB simulations compared to the linear (or bi-linear 'ramping') in the case of MC, significant block rotations are seen with BB which tend to be absent with MC.

Such diverging approaches, coupled with the inherent complexity of jointed rock behavior, have created unfortunate barriers that, to date, have prevented comprehensive and generally accepted approaches to rock mechanics, as needed for solving rock engineering problems. Discontinuum and continuum mechanics approaches are applicable to specific rock mass conditions, and cannot be used interchangeably. The discontinuum approach is appropriate when the geological structure controls anisotropy, deformation modes, and strength. Such conditions are applicable to the vast majority (>90%) of rock masses. The continuum approach is appropriate where the frequency and orientation of jointing are such that no preferential paths of stress-strain responses are present. Such conditions are present in an estimated <10% of rock masses. It should be noted that these estimates are based on the observations and interpretations of the authors regarding the influence of geologic structure in numerous cases over decades of experience from hundreds of projects in several dozen countries.

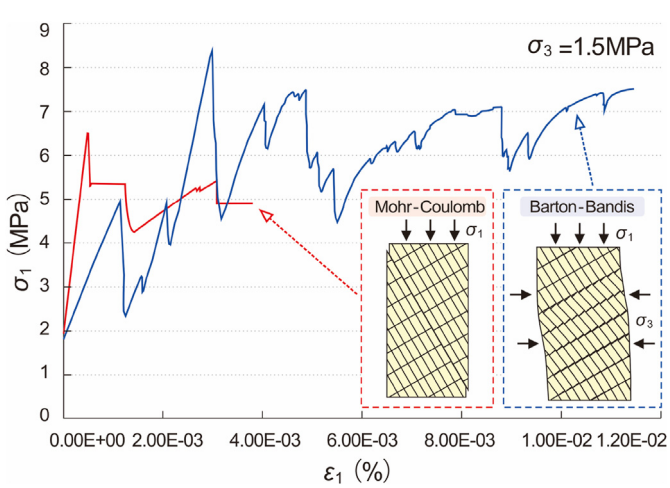

Fig. 25. Contrasting simulation result based on the nonlinear BB and the linear MC criteria (modeling by Bandis, in Barton and Bandis, 2017).

The term 'modeling' (in the case of discontinua) is used to describe the basic stress-displacement-dilation behavior of joints in shear, and the basic stress-closure behavior when joints are compressed by increased effective normal stress. These are the basic elements of the (nonlinear) behavior, which are used when modeling the 2D or 3D behavior of a jointed rock mass. They are the basic BB (Barton-Bandis) components of any UDEC-BB distinct element numerical model. The BB approach can also be used to determine improved MC (Mohr-Coulomb) strength components for a 3DEC-MC 3D distinct element numerical model.

8.2. JRC related engineering applications

The concept of *JRC* has the advantage of being simple, making it easy to perform the necessary tilt tests in the laboratory for small samples while explicitly considering the scale effect (Jing and Hudson, 2004). The Barton-Bandis (BB or *JRC-JCS*) joint model, providing a nonlinear shear strength envelope for rock joints, has been widely applied in rock engineering practices, such as the rock slope stability, underground openings, and hydraulic engineering.

8.2.1. Rock slope stability

The stability of rock slopes is influenced by many factors, such as stress conditions, joint distributions, drainage of water, and the mechanical properties of the rock mass. Among the above-mentioned factors, the existence of rock joints usually represents the weak spots controlling both the stability and the potential failure mode of the rock slopes. This is because the shear strength of the rock joints is usually low compared to the intact rocks (Bye and Bell, 2001; Duzgun and Bhasin, 2009). Thus, the BB model has been successfully applied in estimating the shear strength of rock joints to accurately evaluate the stability of the slopes.

Many researchers examined the effectiveness of the BB model through direct shear tests and rockslide back analysis (Wines and Lilly, 2003; Chiliza and Hingston, 2018). These examinations confirmed that the BB model can satisfactorily predict the shear strength of rock joints and closely represents the actual physical characteristics of the slopes (Grøneng et al., 2009; Zhao et al., 2020). Researchers also confirmed that the UDEC-BB presented good performance in assessing the stability and deformation characteristics of rock slopes (Kim et al., 2013). Moreover, the BB model has been employed in probabilistic methods to improve the reliability of the slope stability analysis results (Kveldsvik et al., 2008; Zhao et al., 2016). A method for assessing slope stability in large open-pit mines was recently provided by Du et al. (2022b), and it was based on a thorough analysis of the geometry and shear strength of the geological discontinuities. They emphasized the significance of accurately describing all geometric aspects of geological discontinuities, particularly their spatial distributions and sizes on step-shaped slopes. The geographical positions of the rock discontinuities, and the size of the rock joints should be matched to specific and relevant locations in the slope. Good estimates of the shear strength of the potential sliding planes are needed. For in situ testing, excavation is typically too quick, and the availability of laboratory measurements is constrained by economics. The BB model-based field calculation of the shear strength of discontinuities offered a workable approach.

8.2.2. Underground openings

Underground excavations in jointed or faulted rocks probably fail by translational shear on a limited number of discontinuity surfaces. Recognizing the need to improve the M − C and other (nonlinear) shear strength criteria for the intact strength of rock,

Barton (1987) summarized his constitutive model for the shear strength of rock joints as applied in the BB model, which takes into account the scale effect caused by different block sizes. The distinct element numerical method based on the BB model has proved effective in calculating features such as joint shear, joint aperture, and permeability changes resulting from underground excavation. Bhasin and Høeg (1998) performed parametric studies with UDEC-BB for a large cavern in a jointed rock mass. These researchers found that the BB model predicts smaller deformation than the MC model because it allows for the modeling of the subsequent shear-induced dilation and, consequently, the accumulation of larger normal stresses. According to the sensitivity studies, the increase in *JCS for the case of a moderate strength rock* induced a remarkable reduction in the displacements around the opening, and the influence of *JRC* was in this case limited.

In preparation for the 1994 Winter Olympic Games in Norway, a team from NGI performed stress measurements, cross-hole seismic tomography, joint characterization and UDEC-BB modeling, comparing predicted deformations with subsequent MPBX-measured deformations. The work was done as a design check for the owner of the 60 m span planned ice hockey cavern. Results were so close for the bolted and lightly anchored model (predicted maxima 7–9 mm, measured maxima 7–8 mm) that the project can almost be considered as a verification of the UDEC-BB modeling (see Barton et al., 1994 for details). An important proviso is that the fibre-reinforced shotcrete S(fr) was not part of the UDEC-BB model at this time. The S(fr) looks after the details of the rock mass behavior 'between the bolts' such as blast damage and overbreak, but such details were not part of the pre-1990 numerical modeling.

8.2.3. Hydraulic engineering

Dams are usually designed and built to withstand the most severe unstable conditions, including over-topping. In most cases, investigations of failed dams show that these failures are often associated with discontinuities, because they are the preferred planes for deformation and rupture, leading to the collapse of the entire structure. Thus, it is necessary to accurately estimate the shear strength of rock joints existing in dams. Owing to the efficiency and simplicity of the BB model, researchers have used this model to predict the shear strength of rock joints in dams. Based on the predicted shear strength of rock joints, the sliding stability analyses of dams and the spatial variability of shear strength along joints can be successfully performed (Johansson, 2009; Sow et al., 2017). Considering that the *JRC* is a key parameter when using the BB model, some researchers introduced the relationships between the *JRC* and statistical parameters or fractal dimensions to the BB model when analyzing the dam discontinuities (Sanei et al., 2015; Kebab et al., 2021). As the rock joints in dam sites are sometimes not well matched, Renaud et al. (2019) adopted the orientation-dependent *JRC* and *JMC* to investigate the contribution of roughness to the shear strength of a dam foundation joint. Since filled rock joints are frequently encountered in dam foundations, some researchers thoroughly investigated the BB model and modified it to evaluate the shear strength of filled rock joints at the laboratory scale and large scale (Geertsema, 2003; Maleki, 2011). In addition to the filled or unfilled rock joints, the shear mechanism of concrete–rock mass interfaces of dam foundations could also be studied based on the BB model (Andjelkovic et al., 2015).

9. Discussion

9.1. Representativeness of the rock joint samples

The roughness and shear strength of rock joints can sometimes vary dramatically with location, even when measured along the same direction and on the same joint. The heterogeneity is responsible for the spatial variability in the roughness and shear behavior, and researchers usually characterize this property using statistical analysis. Sampling bias may result in incorrect predictions in statistics (Spiegel and Stephens, 2017). Before drawing conclusions about the population, researchers should be aware of the appropriate amount of individual samples they need to collect. However, the representativeness of the rock joint samples has received little attention in previous studies, and there is still no solution to the issue of measuring roughness and shear strength with insufficient sample numbers. For example, it is difficult to accurately characterize the statistical information of the shear strength due to a limited number of samples, for instance, if just 3–5 samples are available for each test series. In this case, the shear tests often yield unrepresentative data. Furthermore, the selection of test samples could have an effect on the observation of scale effects, and sampling bias could result in inaccurate conclusions about the scale effect (Barton, 1990). Unfortunately, the number of test samples utilized in some studies is insufficient for statistically analyzing the influence of scale on shear strength (Yong et al., 2018a), which may lead to failure in the investigation of the scale effect.

Determining the required minimum number (RMN) of test specimens for the desired accuracy of roughness and shear strength is of great interest to obtain the satisfactory accuracy of geotechnical performance estimate with low economic cost. Taking the shear strength of rock joints as an example, the tested specimens are recommended to be taken from the same joint or test horizon with similar characteristics. Considering the difficulties in preparing specimens with similar characteristics, one of the best choices in engineering practice is to adopt the mean shear strength of specimens collected from the population group. For subgroups containing i specimens, the normal distribution for the sample mean μ_i is shown in Fig. 26a. If the acceptable relative error of the population mean μ is set to ε, the probability (P_ε) that the test result of a random subgroup can satisfactorily estimate μ is the area enclosed between the probability density curve and the abscissa axis from μ-ε to μ+ε. The formula to calculate P_ε is

$$P_\varepsilon = \int_{\mu(1-\varepsilon)}^{\mu(1+\varepsilon)} \frac{1}{\sigma\sqrt{2\pi}} e^{-\frac{(\mu_i-\mu)^2}{2\sigma^2}} d\mu_i \tag{39}$$

where σ is the standard deviation of the sample mean μ_i.

Generally, one has confidence in the test results with high P_ε values. If a specified P_ε is required, the relative error ε of the test result of a subgroup can be estimated as follows:

$$\varepsilon = \frac{\sigma}{\mu} z_{(1+P_\varepsilon)/2} \tag{40}$$

where $z_{(1+P_\varepsilon)/2}$ is the upper quantile of the standard normal distribution corresponding to the probability $(1 + P_\varepsilon)/2$.

The number of test specimens to estimate the population mean μ should simultaneously meet the acceptable ε and P_ε. Taking the laboratory-scale rock joint specimens collected from a large slate rock joint as an example, the RMN under different normal stresses for a given acceptable ε and P_ε was calculated. As shown in Fig. 26b, for an acceptable ε and P_ε, the RMN decreases as the normal stress increases. Since the heterogeneity of rock joints decreases with the increases of normal stress and scale, the effective sampling numbers of rock joints to accurately characterize the roughness and shear strength will decrease for larger rock joints.

Since the shear strength and the value of JRC are positively correlated, this suggests that the scale effects of shear behavior and

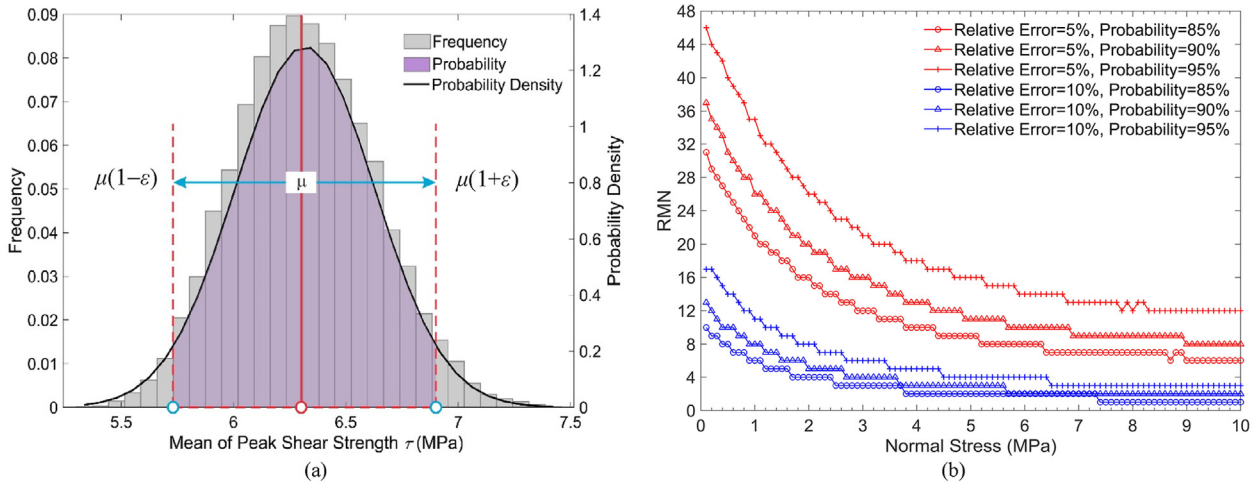

Fig. 26. (a) Sketch to determine the probability of the sample mean of shear strength deviating from the population mean of shear strength within a relative error, and (b) Required minimum number (RMN) of specimens to estimate the shear strength as the normal stress increases.

surface roughness are tightly related (Du et al., 2011). Yong et al. (2018a) proposed an overlapping sampling method to address the sampling problem in studies of scale effects. The effective sampling number of joint samples of different sizes is determined according to the analysis of the coefficient of variation (CV) by the class ratio method. They propose that a representative sample can be obtained by selecting a sample whose roughness is close to the maximum likelihood estimate of the probability distribution of roughness. The following equation is suggested for the quantification of the representativeness of each sample:

$$\eta_i = \frac{|JRC_i - \theta|}{\theta} \times 100\% \tag{41}$$

where η_i and JRC_i denote the representativeness and the *JRC* value of joint sample *i*, respectively; and θ represents the mean value of the roughness. By doing so, it is possible to identify the most representative sample when η_i reaches the minimum value. To obtain enough sample capacity for representative sampling, Huang et al. (2020) developed the progressive coverage statistical approach based on the stratified sampling theory. According to the sampling result, they made multiscale (100 mm × 100 mm–1000 mm × 1000 mm) joint replicas and conducted the multiscale direct shear test to investigate the scale effect on shear strength. Considering the accessibility of the plane of interest, the area of the exposed part of the potential sliding plane that satisfies the measurement conditions is usually limited. It brings challenges to collecting sufficient samples to study joint roughness characteristics.

To overcome the potential sampling problem, Du et al. (2022a) developed the global search method (GSM), and based on this, a method to determine the most representative samples was proposed. By using this method, exclusive sampling results (all the samples at different locations) can be provided, avoiding sampling bias existing in conventional sampling methods due to the personal judgment of the researcher. For example, using the equal-partition sampling method (EPSM), we can only obtain ten 100 mm long samples over the entire length $L = 1000$ mm of a natural joint, while all individual samples (1801 in total) can be obtained using GSM. By doing so, the roughness heterogeneity can be systematically characterized based on the analysis of *JRC*. Fig. 27 compares the distribution of the *JRC* values using different sampling methods. Although the obtained JRC_{mean} using EPSM is consistent with the result by GSM, there is a clear difference between the obtained $JRC_{St.Dev}$. The *JRC* values in the range 12–14 reached the highest relative frequencies in Fig. 27a, but there is no data for *JRC* values in the same range in Fig. 27b. It can be seen that the main advantage of the GSM is that the sampling results are systematic and reproducible.

In addition, for each joint profile with a length of 1000 mm, we can obtain ten joint samples with a length of 100 mm or two samples with a length of 500 mm using EPSM. The above discussion has proved that the samples obtained by EPSM are insufficient for the statistical analysis of the roughness of the 100 mm joint samples. Here, we explain this topic further using based on the 500 mm long samples. The 500 mm long samples were obtained from the profiles (P_{01}, P_{02}, …, and P_{51}) in Fig. 28 using both GSM and EPSM. Then, the JRC_{mean} values of the samples taken from each profile were calculated.

Fig. 29 illustrates that JRC_{mean} presents apparent differences between the values obtained by GSM and EPSM. For each profile, different samples can be extracted from different locations using GSM, and the total number of the samples is 1001. However, only two samples can be extracted from each profile using EPSM. As shown in Fig. 29, the values of JRC_{mean} of the samples obtained from the profiles P_{01} to P_{31} are underestimated, but the values of the samples obtained from the profiles P_{32} to P_{51} are overestimated. The largest relative error is 32.59%. Therefore, JRC_{mean} of 500 mm joint samples by EPSM also failed to represent the overall roughness.

9.2. Sampling interval

For roughness measurement-based *JRC* estimation, researchers need to quantify the roughness based on discrete points along the joint surfaces obtained under a certain sampling interval (*SI*) (Yu and Vayssade, 1991; Zhou and Xie, 2004; Tatone and Grasselli, 2010; Yan et al., 2020). The digitized profiles with larger *SI* are usually smoother than those profiles digitized using smaller *SI*. This is because the unevenness between adjacent data points is smoothed with larger *SI*. Thus, how to choose the appropriate *SI* value should be paid enough attention; otherwise, it may lead to uncertainty in *JRC* estimation. Yong et al. (2018a) proposed a method for determining the maximum sampling interval (SI_{max}) based on the Fourier series. The Fourier series has been proven effective in decomposing a joint profile into some periodic functions, which has been widely adopted in quantifying the joint

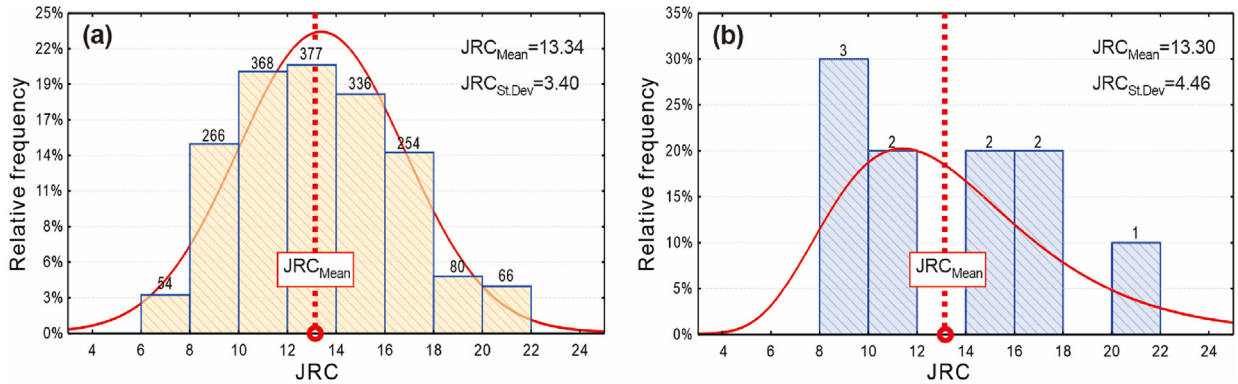

Fig. 27. Comparison of the distribution of the *JRC* values using different sampling methods: (a) GSM and (b) EPSM (after Du et al., 2022a).

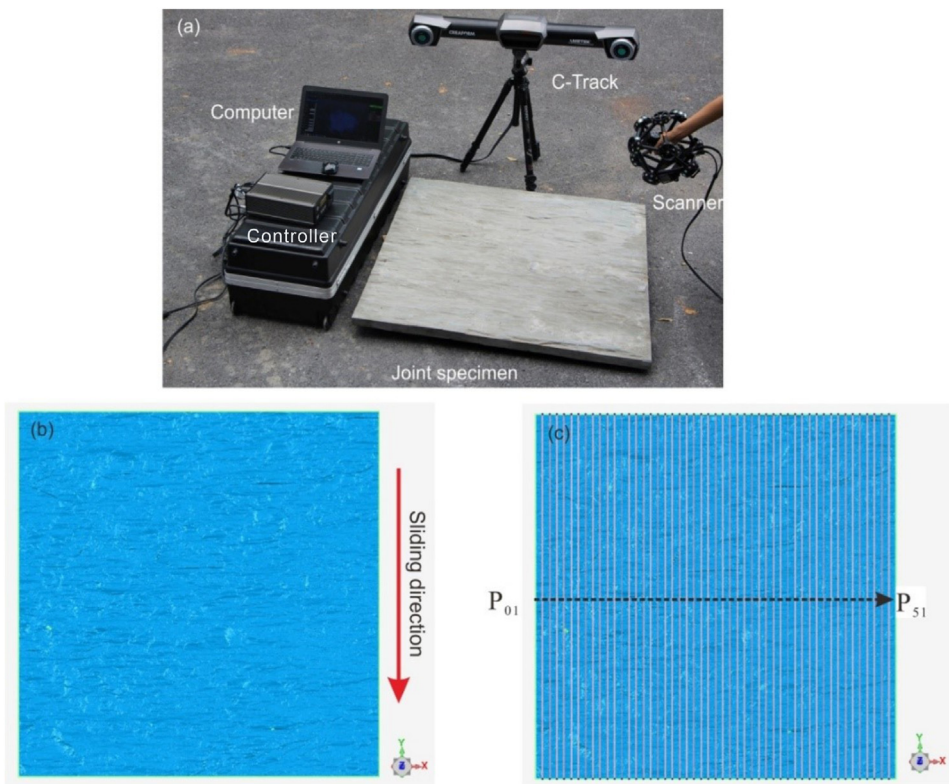

Fig. 28. Generation of the joint surface digitization (after Du et al., 2022a): (a) Scanning of the joint surface, (b) Digitized joint surface, and (c) Locations of the digitized profiles.

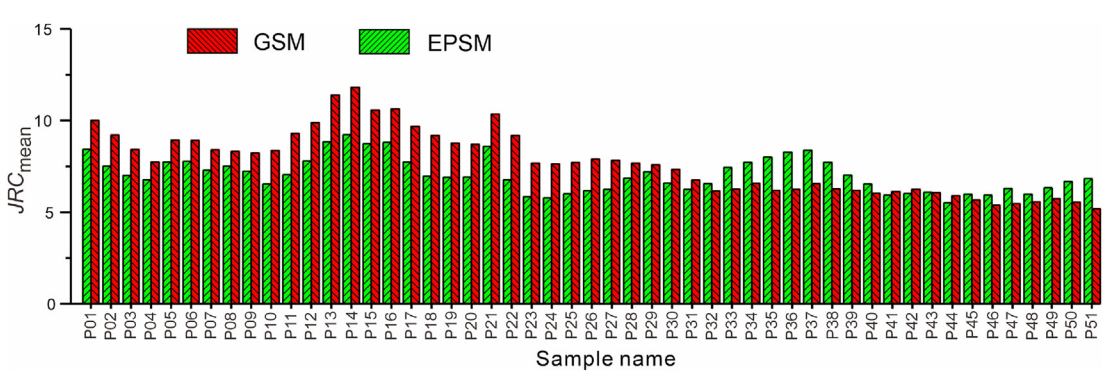

Fig. 29. Comparison of the values of JRC_{mean} of 500 mm long joint samples by GSM and EPSM (after Du et al., 2022a).

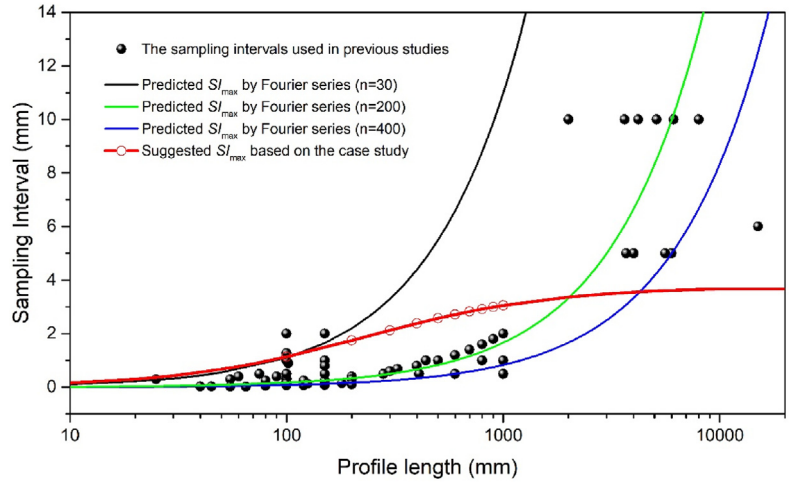

Fig. 30. Comparison of the *SI* applied in some previous studies and the predicted SI_{max} under different approximation levels (after Yong et al., 2018b).

roughness (Yang et al., 2001, 2010; Zheng and Qi, 2016). As shown in Fig. 30, there is a positive correlation between the *SI* and the sample sizes. The roughness measurements on small samples require smaller *SI* to achieve higher measurement resolution, while larger *SI* values were suggested for measuring large-scale joint samples. Based on the Fourier series and Shannon's sampling theorem, the suggested values of SI_{max} under different approximation levels were predicted. They found that most of the *SI* used in many previous studies are smaller than the SI_{max} for laboratory-sized joints (<1 m^2). Nevertheless, the SI values for studying the roughness of field-scale joints (≥ 1 m^2) are generally too large (Fig. 30).

Bao et al. (2020) found that as the *SI* increases, there is a distinct threshold beyond which the *JRC* value changes from constant to variable. According to their study, the *JRC* value keeps constant if the profile line *SI* is smaller than 4 mm, which is independent of the joint roughness. However, the threshold of digital point SI is influenced by joint roughness and has a negative exponential relationship with the *JRC* value. Huan et al. (2021) established the functional relationships between the statistical parameters and *JRC* under various *SI* and noted that the *JRC* prediction accuracy would be reduced with the increase of *SI*. Ge et al. (2021) investigated the influences of roughness level on the appropriate *SI*, which was suggested to be determined based on the inflection point with the maximum curvature on the curves of *SI* vs. roughness coefficient. These studies enriched avenues for roughness measurement-based *JRC* estimation for laboratory-sized joints. It should be emphasized that more attention should be paid to determining the suitable *SI* required for rock joint roughness measurements at the field scale.

10. Conclusions

The concept of *JRC* stems from Barton (1973)'s work with rock joints which provides a solution to nonlinear shear strength. It has been 50 years since it was first proposed. The simple form of *JRC* provides for improved communication and also provides input for modeling behavior (e.g. shear strength, dilation, joint permeability, and permeability-change). Numerous research results clearly show that *JRC* is a crucial parameter for the quantitative description of rock joint surface geometry status and one of the most important variables in accurately forecasting the shear strength of joints.

There are many profile-related equations in the literature, and hundreds of articles, all addressing *JRC*. Many do not reference the source of *JRC* anymore, assuming it is an 'established parameter'. However, it is sometimes criticized and misunderstood. Many researchers quite reasonably criticized the *JRC* estimation by visual comparison to ten standard profiles. In fact, the purpose of these standard profiles with suggested ranges of *JRC* like 8 to 10, and 14 to 16, was to show the variation in the roughness of the 130 joint samples tested by Barton and Choubey (1977). The tilt test method is still one of the most 'scientific' ways to determine *JRC*, but unfortunately, it seems to be neglected in the great majority of 'improving *JRC*' studies.

Joint roughness is complicated because it includes characteristics such as anisotropy and scale effects. Despite all of the progress made, the distinctive and quantitative characterization of *JRC* and its conclusive connections with hydro-mechanical parameters of fractures remain a great challenge. There appears to be plenty of room for further investigation, so that the uncertainty in *JRC* estimation can be systematically investigated. There is also an urgent need to more accurately determine the relationship between *JRC* and the size of rock joint samples larger than 10 m. To these could be added more research into the importance of block-size, or the spacing of cross-joints.

We must not neglect 'joints and geology' in the practice of rock mechanics modeling and understanding. The *JRC*-related constitutive modeling method, the BB model, is an accurate nonlinear equation that is widely used in rock mechanics, especially when a wide variety of stress is involved. UDEC-BB modeling is recommended to emphasize the possibility of representing some details of 'geology and structure' at least in 2D, and more focus needs to be paid to in situ measurement and statistical incorporation into discontinuum (jointed) modeling codes like a hoped-for '3DEC-BB'.

Declaration of competing interest

The authors declare that they have no known competing financial interests or personal relationships that could have appeared to influence the work reported in this paper.

Acknowledgments

The study was funded by the National Natural Science Foundation of China (Grant Nos. 42177117 and 42207175), Zhejiang Provincial Natural Science Foundation (Grant No. LQ16D020001). We must all thank Bandis (†) for his unparalleled contribution to the study of the mechanical behavior of rock joints.

References

Alameda-Hernández, P., Jiménez-Perálvarez, J., Palenzuela, J.A., Hamdouni, R.E., Irigaray, C., Cabrerizo, M.A., Chacón, J., 2014. Improvement of the JRC calculation using different parameters obtained through a new survey method applied to rock discontinuities. Rock Mech. Rock Eng. 47, 2047–2060.

Andjelkovic, V., Pavlovic, N., Lazarevic, Z., Nedovic, V., 2015. Modelling of shear characteristics at the concrete–rock mass interface. Int. J. Rock Mech. Min. 76, 222–236.

Bae, D.S., Kim, K.S., Koh, Y.K., Kim, J.Y., 2011. Characterization of joint roughness in granite by applying the scan circle technique to images from a borehole televiewer. Rock Mech. Rock Eng. 44 (4), 497–504.

Bahaaddini, M., Serati, M., Khosravi, M.H., et al., 2022. Rock joint micro-scale surface roughness characterisation using photogrammetry method. J. Min. Environ. 13 (1), 87–100.

Bandis, S.C., 1980. Experimental Studies of Scale Effects on Shear Strength and Deformation of Rock Joints. PhD Thesis. Department of Earth Sciences, University of Leeds.

Bandis, S.C., Lumsden, A.C., Barton, N.R., 1981. Experimental studies of scale effects on the shear behaviour of rock joints. Int. J. Rock Mech. Min. Sci. Geomech. Abstr. 18, 1–21.

Bandis, S.C., Makurat, A., Vik, G., 1985. Predicted and measured hydraulic conductivity of rock joints. In: Proceedings of International Symposium on Fundamentals of Rock Joints, pp. 269–280. Bjørkliden, Sweden.

Bao, H., Zhang, G.B., Lan, H.X., Yan, C.G., Xu, J.B., Xu, W., 2020. Geometrical heterogeneity of the joint roughness coefficient revealed by 3D laser scanning. Eng. Geol. 265, 105415.

Barton, N.R., 1971. A relationship between joint roughness and joint shear strength. In: Proceedings of the International Symposium on Rock Mechanics. Nancy, France, pp. 1–8.

Barton, N.R., 1972. A model study of air transport from underground openings situated below groundwater level. In: Proceedings of the Symposium of International Society for Rock Mechanics, Percolation through Fissured Rock. Stuttgart, Theme 3A.

Barton, N.R., 1973. Review of a new shear-strength criterion for rock joints. Eng. Geol. 7, 287–332.

Barton, N.R., 1976. The shear strength of rock and rock joints. Int. J. Rock Mech. Min. Sci. Geomech. Abstr. 13, 255–279.

Barton, N.R., 1978. Suggested methods for the quantitative description of discontinuities in rock masses. Int. J. Rock Mech. Min. Sci. Geomech. Abstr. 15 (6), 319–368.

Barton, N.R., 1981. Shear strength investigations for surface mining. In: Proceedings of the 3rd International Conference on Surface Mining. SME, Vancouver, pp. 171–196.

Barton, N.R., 1982. Modelling Rock Joint Behavior from in Situ Block Tests: Implications for Nuclear Waste Repository Design. ONWI-308. prepared by Terra Tek, Inc. for. Office of Nuclear Waste Isolation, Battelle Memorial Institute, Columbus, OH.

Barton, N.R., 1987. Predicting the behaviour of underground openings in rock. In: 4th Manual Rocha Memorial Lecture, pp. 1–21. Lisbon.

Barton, N.R., 1990. Scale effects or sampling bias? Closing Lecture. In: Pinto, da Cunha (Ed.), Scale Effects in Rock Masses, pp. 31–55. Rotterdam.

Barton, N.R., 1991. Geotechnical Design. World Tunn. November, pp. 410–416.

Barton, N.R., 1999. General Report Concerning Some 20th Century Lessons and 21st Century Challenges in Applied Rock Mechanics, Safety and Control of the Environment. 9th ISRM Congress, Paris, France, pp. 1659–1679.

Barton, N.R., 2002. Some new Q-value correlations to assist in site characterization and tunnel design. Int. J. Rock Mech. Min. Sci. 39 (2), 185–216.

Barton, N.R., 2006. Rock Quality, Seismic Velocity, Attenuation and Anisotropy, 1st ed. CRC Press, London.

Barton, N.R., 2013. Shear strength criteria for rock, rock joints, rockfill and rock masses: problems and some solutions. J. Rock Mech. Geotech. Eng. 5 (4), 249–261.

Barton, N.R., 2020. A review of mechanical over-closure and thermal over-closure of rock joints: potential consequences for coupled modelling of nuclear waste disposal and geothermal energy development. Tunn. Undergr. Space Technol. 99, 103379.

Barton, N.R., 2021. New ideas about failure modes in rock masses – from tunnels to Prekestolen to El Capitan to Everest. Bergmekanikkdag 33, 1–33.20. Oslo.

Barton, N.R., Bakhtar, K., 1983. Bolt design based on shear strength. In: Proceedings of International Symposium on Rock Bolting, pp. 367–376. Abisko, Sweden.

Barton, N.R., Bakhtar, K., 1987. Description and Modelling of Rock Joints for the Hydro-Thermal-Mechanical Design of Nuclear Waste Vaults. Atomic Energy of Canada Limited. TR-418. vols. I and II.

Barton, N.R., Bandis, S.C., 1982. Effects of block size on the shear behavior of jointed rock. keynote lecture. In: 23rd U.S. Symposium on Rock Mechanics, pp. 739–760. Berkely, California.

Barton, N.R., Bandis, S.C., 2017. Characterization and modelling of the shear strength, stiffness and hydraulic behaviour of rock joints for engineering purposes. In: Feng, X.T. (Ed.), Rock Mechanics and Engineering, 1st ed. CRC Press, pp. 3–40.

Barton, N.R., Bar, N., 2015. Introducing the Q-Slope Method and its Intended Use within Civil and Mining Engineering Projects. Geomechanics Colloquium, pp. 157–162.

Barton, N.R., Choubey, V., 1977. The shear strength of rock joints in theory and practice. Rock Mech. 1/2, 1–54.

Barton, N.R., Hansteen, H., 1979. Very Large Span Openings at Shallow Depth: Deformation Magnitudes from Jointed Models. RETC, Atlanta, pp. 1–23.

Barton, N.R., Quadros, E., 1997. Joint aperture and roughness in the prediction of flow and groutability of rock masses. Int. J. Rock Mech. Min. Sci. 34 (3–4), 252.

Barton, N.R., Quadros, E., 2015. Anisotropy is everywhere, to see, to measure, and to model. Rock Mech. Rock Eng. 48 (4), 1323–1339.

Barton, N.R., Quadros, E., 2019. Understanding the need for pre-injection from permeability measurements: what is the connection? J. Rock Mech. Geotech. Eng. 11 (3), 576–597.

Barton, N.R., Shen, B., 2018. Extension strain and rock strength limits for deep tunnels, cliffs, mountain walls and the highest mountains. Rock Mech. Rock Eng. 51 (12), 3945–3962.

Barton, N.R., Lien, R., Lunde, J., 1974. Engineering classification of rock masses for the design of tunnel support. Rock Mech. Rock Eng. 6 (4), 189–236.

Barton, N.R., Bandis, S.C., Bakhtar, K., 1985. Strength, deformation and conductivity coupling of rock joints. Int. J. Rock Mech. Min. Sci. Geomech. Abstr. 22 (3), 121–140.

Barton, N.R., By, T.L., Chryssanthakis, P., et al., 1994. Predicted and measured performance of the 62 m span Norwegian Olympic ice hockey cavern at Gjøvik. Int. J. Rock Mech. Min. Sci. Geomech. Abstr. 31 (6), 617–641.

Beer, A.J., Stead, D., Coggan, J.S., 2002. Estimation of the joint roughness coefficient (JRC) by visual comparison. Rock Mech. Rock Eng. 35, 65–74.

Bhasin, R., Høeg, K., 1998. Parametric study for a large cavern in jointed rock using a distinct element model (UDEC—BB). Int. J. Rock Mech. Min. Sci. 35 (1), 17–29.

Bhasin, R., Johansen, P.M., Barton, N.R., Makurat, A., 2002. Rock joint sealing experiments using an ultra fine cement grout. In: Proceedings of the North American Tunneling Conference (Seattle).

Bieniawski, Z.T., 1973. Engineering classification of jointed rock masses. Trans. S. Afr. Inst. Civ. Eng. 15, 335–344.

Bjurström, S., 1974. Shear strength of hard rock joints reinforced by grouted intensional bolts. In: Proceedings of 3rd International Congress on Rock Mechanics, pp. 1194–1199.

Broch, E., Franklin, J.A., 1972. The point-load strength test. Int. J. Rock Mech. Min. Sci. Geomech. Abstr. 9 (6), 669–676.

Brown, S.R., Scholz, C.H., 1985. Closure of random elastic surfaces in contact. J. Geophys. Res. Solid Earth 90 (B7), 5531–5545.

Buzzi, O., Casagrande, D., 2018. A step towards the end of the scale effect conundrum when predicting the shear strength of large in situ discontinuities. Int. J. Rock Mech. Min. Sci. 105, 210–219.

Bye, A.R., Bell, F.G., 2001. Stability assessment and slope design at Sandsloot open pit, South Africa. Int. J. Rock Mech. Min. Sci. 38 (3), 449–466.

Cecil III, O.S., 1970. Correlations of Rock Bolt-Shotcrete Support and Rock Quality Parameters in Scandinavian Tunnels. PhD Thesis. University of Illinois, Urbana.

Chen, S.J., Zhu, W.C., Yu, Q.L., Liu, X.G., 2015. Characterization of anisotropy of joint surface roughness and aperture by variogram approach based on digital image processing technique. Rock Mech. Rock Eng. 49, 855–876.

Chen, J.Q., Ye, J., Du, S.G., 2017a. Scale effect and anisotropy analyzed for neutrosophic numbers of rock joint roughness coefficient based on neutrosophic statistics. Symmetry 9 (10), 208.

Chen, J.Q., Ye, J., Du, S.G., Yong, R., 2017b. Expressions of rock joint roughness coefficient using neutrosophic interval statistical numbers. Symmetry 9 (7), 123.

Chen, N., Zhang, X.B., Jiang, Q.H., Feng, X.X., Wei, W., Yi, B., 2018. Shear behavior of rough rock joints reinforced by bolts. Int. J. GeoMech. 18 (1), 04017130.

Chiliza, S.G., Hingston, E.D.C., 2018. Back analysis of an ancient rockslide at lake fundudzi, limpopo Province, South Africa. Bull. Eng. Geol. Environ. 77 (1), 29–47.

Cook, N.G.W., 1992. Natural joints in rock: mechanical, hydraulic and seismic behaviour and properties under normal stress. Int. J. Rock Mech. Min. Sci. Geomech. Abstr. 29 (3), 198–223.

Deere, D.U., 1963. Technical description of rock cores for engineering purpose. Rock Mech. Eng. Geol. 1 (1), 16–22.

Develi, K., Babadagli, T., Comlekci, C., 2001. A new computer-controlled surface-scanning device for measurement of fracture surface roughness. Comput. Geosci. 27 (3), 265–277.

Diaz, M., Kwang, Y.K., Sun, Y., Li, Z., Sehyeok, P., Ki, B.M., 2017. Surface roughness characterization of open and closed rock joints in deep cores using X-ray computed tomography. Int. J. Rock Mech. Min. Sci. 98, 10–19.

Du, S.G., 1992. Simple profile instrument and its application to study joint roughness coefficient of rock. Geol. Sci. Technol. Inf. 11 (3), 91–95.

Du, S.G., 1993. A practical test of JRC estimation by the straight-edge method. In: Proceedings of the 3rd National Youth Symposium on Engineering Geology, pp. 575–579.

Du, S.G., Fan, L.B., 1999. The statistical estimation of rock joint roughness coefficient. Chin. J. Geophys. 42 (4), 577–580.

Du, S.G., Pan, B.T., 1992. Evaluation on slide slope stability of Fengyugou, Xiaolangdi reservoir. Earth Sci. 17 (6), 709–718.

Du, S.G., Chen, Y., Fan, L.B., 1996. Mathematical expression of JRC modified straight edge. J. Eng. Geol. 4 (2), 36–43.

Du, S.G., Yun, J.H., Xiao, F.H., 2009. Measurement of joint roughness coefficient by using profilograph and roughness ruler. J. Earth Sci. 20 (5), 890–896.
Du, S.G., Hu, Y., Hu, X., Guo, X., 2011. Comparison between empirical estimation by JRC-JCS model and direct shear test for joint shear strength. J. Earth Sci. 22 (3), 411–420.
Du, S.G., Du, K.Q., Yong, R., Ye, J., Luo, Z.Y., 2021. Scale effect on the anisotropy characteristics of rock joint roughness. J. Eng. Geol. Hydrogeol. 54 (4), 2020–2066.
Du, S.G., Lin, H., Yong, R., Liu, G.J., 2022a. Characterization of joint roughness heterogeneity and its application in representative sample investigations. Rock Mech. Rock Eng. 55, 3253–3277.
Du, S.G., Saroglou, C., Chen, Y., Lin, H., Yong, R., 2022b. A new approach for evaluation of slope stability in large open-pit mines: a case study at the Dexing Copper Mine. Environ. Earth Sci. 81 (3), 1–21.
Duzgun, H.S.B., Bhasin, R.K., 2009. Probabilistic stability evaluation of Oppstadhornet rock slope, Norway. Rock Mech. Rock Eng. 42 (5), 729–749.
Fardin, N., 2008. Influence of structural non-stationarity of surface roughness on morphological characterization and mechanical deformation of rock joints. Rock Mech. Rock Eng. 41, 267–297.
Fardin, N., Stephansson, O., Jing, L., 2001. The scale dependence of rock joint surface roughness. Int. J. Rock Mech. Min. Sci. 38 (5), 659–669.
Fardin, N., Feng, Q., Stephansson, O., 2004. Application of a new in situ 3D laser scanner to study the scale effect on the rock joint surface roughness. Int. J. Rock Mech. Min. Sci. 41 (2), 329–335.
Ficker, T., Martisek, D., 2016. Alternative method for assessing the roughness coefficients of rock joints. J. Comput. Civ. Eng. 30 (4), 04015059.
Ge, Y., Kulatilake, P.H.S.W., Tang, H., Xiong, C., 2014. Investigation of natural rock joint roughness. Comput. Geotech. 55, 290–305.
Ge, Y., Lin, Z., Tang, H., Zhao, B., 2021. Estimation of the appropriate sampling interval for rock joints roughness using laser scanning. Bull. Eng. Geol. Environ. 80 (6), 3569–3588.
Geertsema, A.J., 2003. The Shear Strength of Rock Joints with Special Reference to Dam Foundations. PhD Thesis. University of Pretoria.
Goodman, R.E., 1970. The deformability of joints. In: Proceedings of Determination of the in Situ Modulus of Deformation of Rock, pp. 174–196.
Goodman, R.E., 1974. The mechanical properties of joints. In: Proceedings of the 3rd International Congress on Rock Mechanics, pp. 127–140. Denver, Colorado.
Grasselli, G., 2001. Shear Strength of Rock Joints Based on Quantified Surface Description. PhD Thesis. Ecole Polytechnique Federale De Lausanne.
Grasselli, G., Egger, P., 2003. Constitutive law for the shear strength of rock joints based on three-dimensional surface parameters. Int. J. Rock Mech. Min. Sci. 40 (1), 25–40.
Grasselli, G., Wirth, J., Egger, P., 2002. Quantitative three-dimensional description of a rough surface and parameter evolution with shearing. Int. J. Rock Mech. Min. 39, 789–800.
Greenwood, J.A., Tripp, J.H., 1970. The contact of two nominally flat rough surfaces. Proc. Inst. Mech. Eng. 185, 625–633.
Greenwood, J.A., Williamson, J.B.P., 1966. Contact of nominally flat surfaces. Proc. R. Soc. A-Math. Phys. Eng. Sci. 295, 300–319.
Grøneng, G., Nilsen, B., Sandven, R., 2009. Shear strength estimation for Åknes sliding area in western Norway. Int. J. Rock Mech. Min. Sci. 46 (3), 479–488.
Hardin, E.L., Barton, N.R., Lingle, R., Board, M.P., Voegele, M.D., 1982. A Heated Flatjack Test Series to Measure the Thermo-Mechanical and Transport Properties of in Situ Rock Masses. Office of Nuclear Waste Isolation, Columbus, Ohio, ONWI, p. 193, 260.
Hencher, S.R., Richards, L.R., 2015. Assessing the shear strength of rock discontinuities at laboratory and field scales. Rock Mech. Rock Eng. 48, 883–905.
Hoek, E., 1994. Strength of rock and rock masses. Int. Soc. Rock Mech. News J. 2 (2), 4–16.
Huan, J., Zhang, Z., He, M., Li, N., 2021. A new statistical parameter for determining joint roughness coefficient (JRC) considering the shear direction and contribution of different protrusions. Adv. Civ. Eng. 2021 1–15.
Huang, X., Qi, S., Xia, K., Shi, X., 2018. Particle crushing of a filled fracture during compression and its effect on stress wave propagation. JGR Solid Earth 123 (7), 5559–5587.
Huang, M., Hong, C.J., Du, S.G., Luo, Z.Y., 2020. Experimental technology for the shear strength of the series-scale rock joint model. Rock Mech. Rock Eng. 53, 5677–5695.
Ishii, E., 2020. A conventional straddle-sliding-packer system as a borehole extensometer: monitoring shear displacement of a fault during an injection test. Eng. Geol. 275, 105748.
Jing, L., Hudson, J.A., 2004. Fundamentals of the hydro-mechanical behaviour of rock fractures: roughness characterization and experimental aspects. Int. J. Rock Mech. Min. Sci. 41 (1), 157–162.
Jing, L., Nordlund, E., Stephansson, O., 1992. An experimental study on the anisotropy and stress-dependency of the strength and deformability of rock joints. Int. J. Rock Mech. Min. Sci. Geomech. Abstr. 29 (6), 535–542.
Johansson, F., 2009. Shear Strength of Unfilled and Rough Rock Joints in Sliding Stability Analyses of Concrete Dam. PhD Thesis. KTH.
Kebab, H., Boumezbeur, A., Rivard, P., 2021. Rock mass properties and their suitability as a foundation for a rolled compacted concrete gravity dam: case study of Beni Haroun dam (Mila, NE Algeria). Bull. Eng. Geol. Environ. 80, 1729–1743.
Kim, D.H., Gratchev, I., Balasubramaniam, A., 2013. Determination of joint roughness coefficient (JRC) for slope stability analysis: a case study from the Gold Coast area, Australia. Landslides 10 (5), 657–664.
Krohn, C.E., Thompson, A.H., 1986. Fractal sandstone pores: automated measurements using scanning-electron-microscope images. Phys. Rev. B 33 (9), 6366.
Kulatilake, P.H.S.W., Balasingam, P., Park, J., Morgan, R., 2006. Natural rock joint roughness quantification through fractal techniques. Geotech. Geol. Eng. 24 (5), 1181–1202.
Kulatilake, P.H.S.W., Du, S.G., Ankah, M.L.Y., et al., 2021. Non-stationarity, heterogeneity, scale effects, and anisotropy investigations on natural rock joint roughness using the variogram method. Bull. Eng. Geol. Environ. 80, 6121–6143.
Kveldsvik, V., Nilsen, B., Einstein, H.H., Nadim, F., 2008. Alternative approaches for analyses of a 100,000 m^3 rock slide based on Barton–Bandis shear strength criterion. Landslides 5 (2), 161–176.
Ladanyi, B., Archambault, G., 1977. Shear strength and deformability of filled indented joints. In: International Symposium on the Geotechnics of Structurally Complex Formations, pp. 317–326. Capri.
Lee, S.D., Harrison, J.P., 2001. Empirical parameters for non-linear fracture stiffness from numerical experiments of fracture closure. Int. J. Rock Mech. Rock. Min. Sci. 38 (5), 721–727.
Lee, H.S., Park, Y.J., Cho, T.F., You, K.H., 2001. Influence of asperity degradation on the mechanical behavior of rough rock joints under cyclic shear loading. Int. J. Rock Mech. Rock Min. Sci. 38 (7), 967–980.
Li, C.C., 2021. Principles and method of rock support for rock burst control. Int. J. Rock Mech. Geotech. Eng. 13 (1), 46–59.
Li, W.F., Bai, J.B., Cheng, J.Y., Peng, S., Liu, H.L., 2015. Determination of coal–rock interface strength by laboratory direct shear tests under constant normal load. Int. J. Rock Mech. Min. Sci. 77, 60–67.
Liu, Q., Tian, Y., Liu, D., Jiang, Y., 2017a. Updates to JRC-JCS model for estimating the peak shear strength of rock joints based on quantified surface description. Eng. Geol. 228, 282–300.
Liu, Q., Tian, Y., Ji, P., Ma, H., 2017b. Experimental investigation of the peak shear strength criterion based on three-dimensional surface description. Rock Mech. Rock Eng. 51, 1005–1025.
Liu, X., Zhu, W., Liu, Y., Yu, Q., Guan, K., 2021. Characterization of rock joint roughness from the classified and weighted uphill projection parameters. Int. J. GeoMech. 21 (5), 04021052.
Liu, X., Zhu, W., Liu, Y., Guan, K., 2022. Reconstruction of rough rock joints: 2D profiles and 3D surfaces. Int. J. Rock Mech. Min. 156, 105113.
Ludvig, B., 1983. Shear tests on rock bolts. In: Proceedings of the International Symposium on Rock Bolting, pp. 113–123.
Magsipoc, E., Zhao, Q., Grasselli, G., 2020. 2D and 3D roughness characterization. Rock Mech. Rock Eng. 53, 1495–1519.
Maiolino, O.S., Pellet, F.L., 2015. Full scale lab testing for the determination of rock bolt contribution to reinforced joint shear strength. In: ISRM Congress 2015, Proceedings of the International Symposium on Rock Mechanics, pp. 1–9.
Malama, B., Kulatilake, P.H.S.W., 2003. Models for normal fracture deformation under compressive loading. Int. J. Rock Mech. Min. Sci. 40 (6), 893–901.
Maleki, M.R., 2011. Study of the engineering geological problems of the havasan dam, with emphasis on clay-filled joints in the right abutment. Rock Mech. Rock Eng. 44 (6), 695–710.
Marache, A., Riss, J., Gentier, S., 2008. Experimental and modelled mechanical behaviour of a rock fracture under normal stress. Rock Mech. Rock Eng. 41 (6), 869–892.
Milne, D., Germain, P., Grant, D., Noble, P., 1991. Systematic rock mass characterization for underground mine design. In: 7th ISRM Congress. OnePetro.
Milne, D., Hawkes, C., Hamilton, C., 2009. A new tool for the field characterization of joint surfaces. In: Proceedings of the 3rd CANUS Rock Mechanics Symposium (Toronto).
Mouzannar, H., Marion, B., Madly, L., Didier, V., 2017. Experimental study of the shear strength of bonded concrete–rock interfaces: surface morphology and scale effect. Rock Mech. Rock Eng. 50 (1), 2601–2625.
Newland, P.L., Allely, B.H., 1957. Volume changes in drained taixial tests on granular materials. Geotechnique 7 (1), 17–34.
Nie, Z., Wang, X., Huang, D., Zhao, L., 2019. Fourier-shape-based reconstruction of rock joint profile with realistic unevenness and waviness features. J. Cent. S. Univ. 26 (11), 3103–3113.
Olson, J.E., Pollard, D.D., 1991. The initiation and growth of en échelon veins. J. Struct. Geol. 13 (5), 595–608.
Olsson, R., Barton, N., 2001. An improved model for hydro-mechanical coupling during shearing of rock joints. Int. J. Rock Mech. Min. Sci. 38, 317–329.
Özvan, A., Dinçer, I., Acar, A., Özvan, B., 2014. The effects of discontinuity surface roughness on the shear strength of weathered granite joints. Bull. Eng. Geol. Environ. 73 (3), 801–813.
Patton, F.D., 1966. Multiple modes of shear failure in rock. In: Proceeding of the 1st Congress of International Society for Rock Mechanics, pp. 509–513.
Peng, S.J., Yue, Y.Q., Liu, Y.X., Xu, J., 2019. Anisotropic characteristics and shear mechanical properties of different genetic structural planes. Rock Soil Mech. 40 (9), 3291–3299 (in Chinese).
Piteau, D.R., 1970. Geological factors significant to the stability of slopes cut in rock. In: Proceedings of Symposium on Planning Open Pit Mines, pp. 33–53. Johannesburg, South Africa.
Pratt, H., Black, A., Brace, W., 1974. Friction and deformation of jointed quartz diorite. In: Proceedings of the 3rd Congress of ISRM, pp. 306–310. Denver, CO.
Renaud, S., Tarik, S., Najib, B., Benjamin, M., Marco, Q., Patrice, R., 2019. Roughness effects on the shear strength of concrete and rock joints in dams based on experimental data. Rock Mech. Rock Eng. 52 (1), 3867–3888.

Please cite this article as: Barton N et al., Advances in joint roughness coefficient (*JRC*) and its engineering applications, Journal of Rock Mechanics and Geotechnical Engineering, https://doi.org/10.1016/j.jrmge.2023.02.002

Ross Brown, D.M., Walton, G., 1975. A portable shear box for testing rock joints. Rock Mech. Rock. Min. 7 (3), 129–153.
Saiang, D., Malmgren, L., Nordlund, E., 2005. Laboratory tests on shotcrete-rock joints in direct shear, tension and compression. Rock Mech. Rock. Min. 38 (4), 275–297.
Sanei, M., Faramarzi, L., Goli, S., Ahmad, F., 2015. Development of a new equation for joint roughness coefficient (JRC) with fractal dimension: a case study of Bakhtiary Dam site in Iran. Arabian J. Geosci. 8 (1), 465–475.
Seidel, J.P., Haberfield, C.M., 1995. Towards an understanding of joint roughness. Rock Mech. Geotech. Eng. 28, 69–92.
Song, J., Yong, R., Zhang, Y., Xu, M., 2021. Statistical similaritya nalysis based on neutrosophic interval probability. Neutrosophic Sets Syst 46 (1), 2–8.
Sow, D., Carvajal, C., Breul, P., et al., 2017. Modeling the spatial variability of the shear strength of discontinuities of rock masses: application to a dam rock mass. Eng. Geol. 220, 133–143.
Spiegel, M.R., Stephens, L.J., 2017. Schaum's Outline of Statistics. McGraw Hill Professional.
Swan, G., 1983. Determination of stiffness and other joint properties from roughness measurements. Rock Mech. Rock Eng. 16 (1), 19–38.
Tang, Z.C., Liu, Q.S., Xia, C.C., Song, Y.L., Huang, J.H., Wang, C.B., 2013. Mechanical model for predicting closure behavior of rock joints under normal stress. Rock Mech. Rock Eng. 47 (6), 2287–2298.
Tanyas, H., Ulusay, R., 2013. Assessment of structurally-controlled slope failure mechanisms and remedial design considerations at a feldspar open pit mine. Western Turkey. Eng. Geol. 155, 54–68.
Tatone, B.S.A., 2009. Quantitative Characterization of Natural Rock Discontinuity Roughness In-Situ and in the Laboratory. Department of Civil Engineering, University of Toronto.
Tatone, B.S.A., Grasselli, G., 2009. A method to evaluate the three-dimensional roughness of fracture surfaces in brittle geomaterials. Rev. Sci. Instrum. 80, 1–10.
Tatone, B.S.A., Grasselli, G., 2010. A new 2D discontinuity roughness parameter and its correlation with JRC. Int. J. Rock Mech. Min. Sci. 47 (8), 1391–1400.
Tian, Y., Liu, Q., Liu, D., Kang, Y., Deng, P., He, F., 2018a. Updates to Grasselli's peak shear strength model. Rock Mech. Rock Eng. 51, 2115–2133.
Tian, Y., Liu, Q., Ma, H., Liu, Q., Deng, P., 2018b. New peak shear strength model for cement filled rock joints. Eng. Geol. 233, 269–280.
Tse, R., Cruden, D.M., 1979. Estimating joint roughness coefficients. Int. J. Rock Mech. Min. Sci. Geomech. Abstr. 16 (5), 303–307.
Ünlüsoy, D., Süzen, M.L., 2020. A new method for automated estimation of joint roughness coefficient for 2D surface profiles using power spectral density. Int. J. Rock Mech. Min. Sci. 125, 1–9.
Wang, L.Q., Wang, C.S., Khoshnevisan, S., Ge, Y.F., Sun, Z.H., 2017. Determination of two-dimensional joint roughness coefficient using support vector regression and factor analysis. Eng. Geol. 231, 238–251.
Wang, C.S., Wang, L.Q., Karakus, M., 2019. A new spectral analysis method for determining the joint roughness coefficient of rock joints. Int. J. Rock Mech. Min. Sci. 113, 72–82.
Wines, D.R., Lilly, P.A., 2003. Estimates of rock joint shear strength in part of the fimiston open pit operation in Western Australia. Int. J. Rock Mech. Min. Sci. 40 (6), 929–937.
Xia, C.C., Yue, Z.Q., Tham, L.G., Lee, C.F., Sun, Z.Q., 2003. Quantifying topography and closure deformation of rock joints. Int. J. Rock Mech. Min. Sci. 40 (2), 197–220.
Xia, C.C., Tang, Z.C., Xiao, W.M., Song, Y.L., 2014. New peak shear strength criterion of rock joints based on quantified surface description. Rock Mech. Rock Eng. 47 (2), 387–400.
Yan, F., Ban, L., Qi, C., Shan, R.L., Yuan, H.H., 2020. Research on the anisotropy, size effect, and sampling interval effect of joint surface roughness. Arabian J. Geosci. 13 (11), 1–9.
Yang, Z., Lo, S., Di, C., 2001. Reassessing the joint roughness coefficient (JRC) estimation using Z_2. Rock Mech. Rock Eng. 34, 243–251.
Yang, Z.Y., Taghichian, A., Li, W.C., 2010. Effect of asperity order on the shear response of three-dimensional joints by focusing on damage area. Int. J. Rock Mech. Min. Sci. 47 (6), 1012–1026.
Yang, W.D., Wang, Y.N., Wang, L., Guo, J.J., 2021. Time-dependent behaviour of clay-concrete interfaces with different contact surface roughnesses under shear loading. Mech. Time-Dependent Mater. 25, 539–564.
Ye, J., Yong, R., Liang, Q.F., Huang, M., Du, S.G., 2016. Neutrosophic functions of the joint roughness coefficient and the shear strength: a case study from the pyroclastic rock mass in Shaoxing City, China. Math. Probl. Eng. 2016, 4825709.
Ye, J., Chen, J.Q., Yong, R., Du, S.G., 2017. Expression and analysis of joint roughness coefficient using neutrosophic number functions. Information 8 (2), 1–13.
Yong, R., Ye, J., Liang, Q.F., Huang, M., Du, S.G., 2017. Estimation of the joint roughness coefficient (JRC) of rock joints by vector similarity measures. Bull. Eng. Geol. Environ. 77 (2), 1–15.
Yong, R., Qin, J., Huang, M., Du, S.G., Liu, J., Hu, G., 2018a. An innovative sampling method for determining the scale effect of rock joints. Rock Mech. Rock Eng. 52 (6), 935–946.
Yong, R., Ye, J., Li, B., Du, S.G., 2018b. Determining the maximum sampling interval in rock joint roughness measurements using Fourier series. Int. J. Rock Mech. Min. Sci. 101, 78–88.
Yong, R., Gu, L.Y., Ye, J., et al., 2019. Neutrosophic function with NNs for analyzing and expressing anisotropy characteristic and scale effect of joint surface roughness. Math. Probl. Eng. 2019, 8718936.
Yong, R., Huang, L., Hou, Q., Du, S.G., 2020. Class ratio transform with an application to describing the roughness anisotropy of natural rock joints. Adv. Civ. Eng. 2020, 5069627.
Yu, X., Vayssade, B., 1991. Joint profiles and their roughness parameters. Int. J. Rock Mech. Min. Sci. Geomech. Abstr. 28 (4), 333–336.
Zhao, J., 1997. Joint surface matching and shear strength. Part B. JRC-JMC shear strength criterion. Int. J. Rock Mech. Min. Sci. 34 (2), 179–185.
Zhao, L., Zuo, S., Li, L., Li, Y.L., Zhang, Y.S., 2016. System reliability analysis of plane slide rock slope using Barton-Bandis failure criterion. Int. J. Rock Mech. Min. Sci. 88, 1–11.
Zhao, Y.F., Zhang, H.T., Nie, Y., 2019. Study of shear capacity of jointed rock mass with prestressed anchor bolt. Adv. Civ. Eng. 2019, 6824543.
Zhao, L., Yu, C., Cheng, X., Zuo, S., Jiao, K.F., 2020. A method for seismic stability analysis of jointed rock slopes using Barton-Bandis failure criterion. Int. J. Rock Mech. Min. Sci. 136, 104487.
Zheng, B., Qi, S., 2016. A new index to describe joint roughness coefficient (JRC) under cyclic shear. Eng. Geol. 212, 72–85.
Zheng, B., Qi, S., Luo, G., Liu, F., Huang, X., Guo, S., 2021. Characterization of discontinuity surface morphology based on 3D fractal dimension by integrating laser scanning with ArcGIS. Bull. Eng. Geol. Environ. 80, 2261–2281.
Zhou, H.W., Xie, H., 2004. Anisotropic characterization of rock fracture surfaces subjected to profile analysis. Phys. Lett. 325 (5–6), 355–362.
Zoorabadi, M., Carter, T.G., 2022. Assessment of concrete-rock contact shear behaviour based on in situ shear tests. Dams Reservoirs 32 (2), 83–92.

Nick Barton was born in 1944 in England. He obtained a BSc degree in Civil Engineering from King's College in 1966, and a PhD concerning shear strength and rock slope stability from Imperial College in 1971. He worked for two long periods at NGI in Oslo between 1971 and 2000, eventually as Division Director and then as Technical Advisor. He also worked for four years at TerraTek (subsequently Schlumberger) in Salt Lake City, and was Manager of Geomechanics from 1981 to 1984. Since 2000 he has had his own international rock engineering consultancy, Nick Barton & Associates, based in Oslo and São Paulo. He has consulted on hundreds of rock engineering projects in a total of 40 countries during 50 years, has 270 publications as first or single author, and has written two books, one on TBM prognosis, the other linking rock quality and seismic attributes of rock masses at all scales. He has 13 international awards including the 6th Müller Lecture of the International Society for Rock Mechanics (ISRM). He developed the widely used *Q*-system for classifying rock masses, and for selecting rock tunnel and cavern single-shell support in 1974. He was originator of the rock joint shear strength parameters *JRC* and *JCS* and co-developer of the resulting Barton-Bandis constitutive laws for rock joint modelling in 1982, which was incorporated as a sub-routine in UDEC-BB in 1985. He also developed the Q_{TBM} prognosis method and Q_{SLOPE} for selecting maintenance-free rock slope bench-face angles. His chief areas of consulting activity have been in hydropower tunnelling and cavern construction, nuclear waste disposal site characterization, metro tunnels and caverns, and site characterization at high dams. He has given more than 50 keynote lectures in international conferences.

Please cite this article as: Barton N et al., Advances in joint roughness coefficient (*JRC*) and its engineering applications, Journal of Rock Mechanics and Geotechnical Engineering, https://doi.org/10.1016/j.jrmge.2023.02.002